PRAMANA
—journal of
physics

© Printed in India

Vol. 48, No. 4,
April 1997
pp. 891–922

A stochastic model for solidification II. Application to binary metallic melts

SHOBHA DASS, GAUTAM JOHRI* and LAKSHMAN PANDEY*
Govt. M. H. College of Science and Home Science, Jabalpur 482 002, India
*Department of Post Graduate Studies and Research in Physics, Rani Durgavati University, Jabalpur 482 001, India

MS received 8 November 1995

Abstract. A stochastic model to study the solidification process developed in part I is applied to various binary alloys having different values of interaction energies. The results obtained for the time evolution of temperature and concentration, rate of growth and shape of the solid–liquid interface are presented.

Keywords. Stochastic; solidification; binary melt.

PACS No. 81·10

1. Introduction

The properties of materials are governed to a large extent by their microstructure which in turn is greatly influenced by the solidification process and the kinetics at the solid–liquid interface. A correlation between solidification parameters and the resulting microstructure must be known to produce materials having desired and reproducible properties.

So far the theoretical approach to solidification phenomenon has been confined mostly to the construction of equilibrium phase diagrams [1–3]. Whereas during solidification the system is far from thermodynamic equilibrium. Nonequilibrium thermodynamics was used by Caroli *et al* [4] to study solidification. The concept of kinetic phase diagrams using a stochastic approach was developed by Chvoj [5–8] to describe processes where equilibrium phase diagrams cannot be used. However Chvoj's model does not include interdependence of temperature and concentration. Also it has not been solved for a binary system in three-dimensions (2-space, 1-time). A three-dimensional (2-space, 1-time) model describing the solidification of binary melts is given in the preceding paper alongwith the analysis and numerical scheme to solve the resulting coupled equations. In this paper the results obtained for six representative systems having different values of interaction energies are given.

2. The model

A solid can be grown from the melt if the melt is below its equilibrium melting temperature. Departure from the equilibrium is always required for the solidification

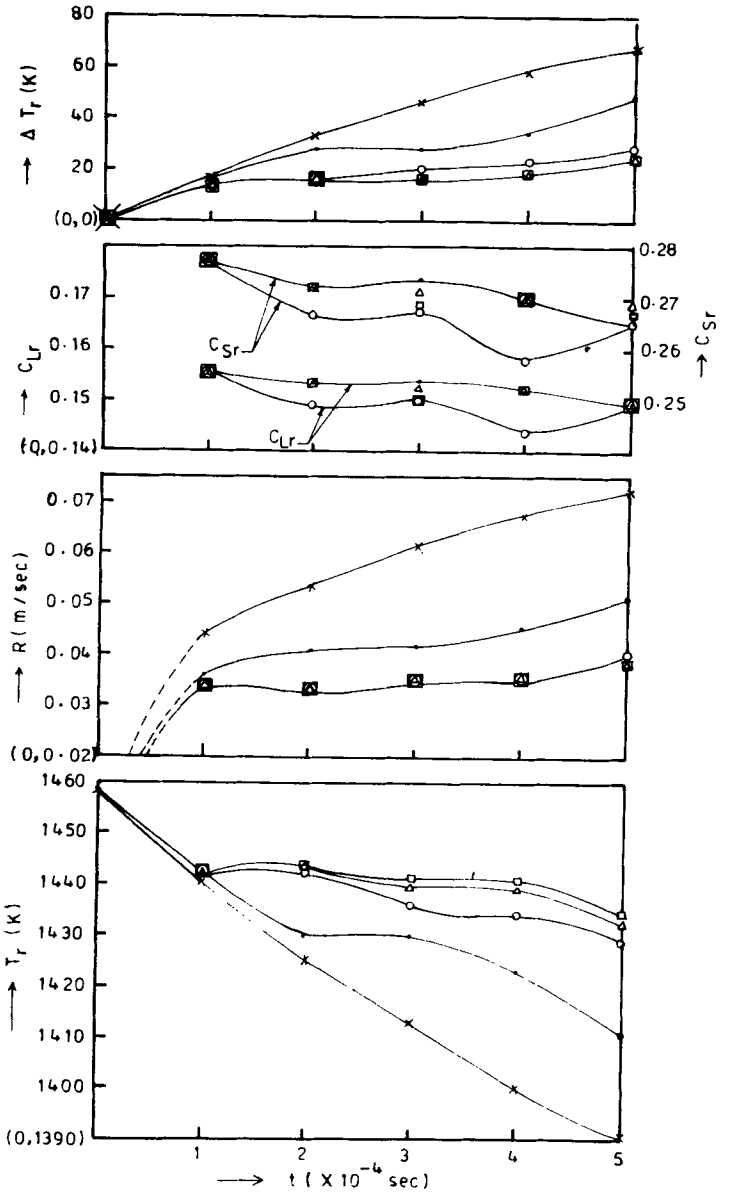

Figure 1. Variation of T_r, R, C_{Lr}, C_{Sr} and ΔT_r with time at (1) $y = 0$ (∗–∗–∗), (2) $y = g$ (•–•–•), (3) $y = 4g$ (o–o–o), (4) $y = 7g$ (△-△-△), (5) $y = 10g$ (□-□-□) for a system with $C_{L0} = 0{\cdot}2$, $T_1 = 1458\,\text{K}$, $\Omega_L = 2{\cdot}8 \times 10^{-20}\,\text{J/atom}$, $\Omega_S = 2{\cdot}33 \times 10^{-20}\,\text{J/atom}$.

process to proceed. The equations describing the formation of solid from a binary melt taking into account the diffusion of mass and heat, thermal and density fluctuations governed by stochastic laws, evolution of latent heat at the solid–liquid interface and the

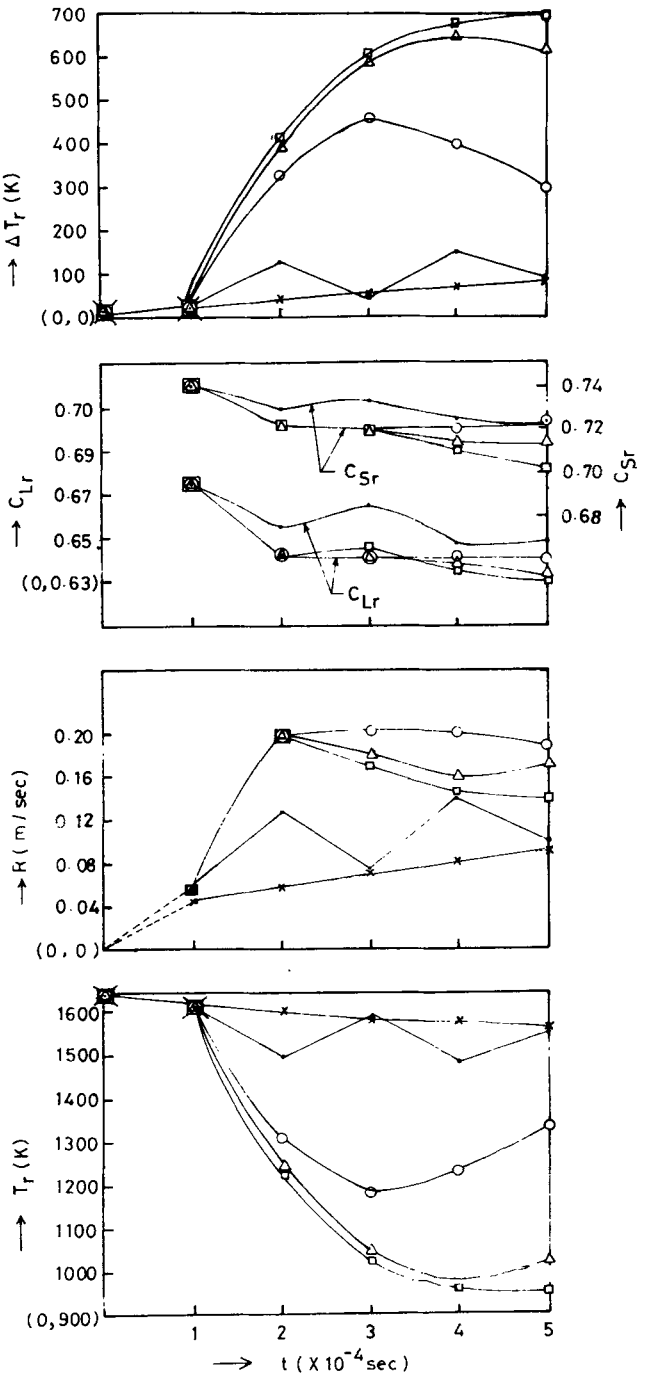

Figure 2. Variation of T_r R, C_{Lr}, C_{Sr} and ΔT_r with time at (1) $y = 0$ (*–*–*), (2) $y = g$ (•–•–•), (3) $y = 4g$ (o–o–o), (4) $y = 7g$ (△-△-△), (5) $y = 10g$ (□-□-□) for a system with $C_{L0} = 0{\cdot}7$, $T_1 = 1643$ K, $\Omega_L = 2{\cdot}8 \times 10^{-20}$ J/atom, $\Omega_S = 2{\cdot}33 \times 10^{-20}$ J/atom.

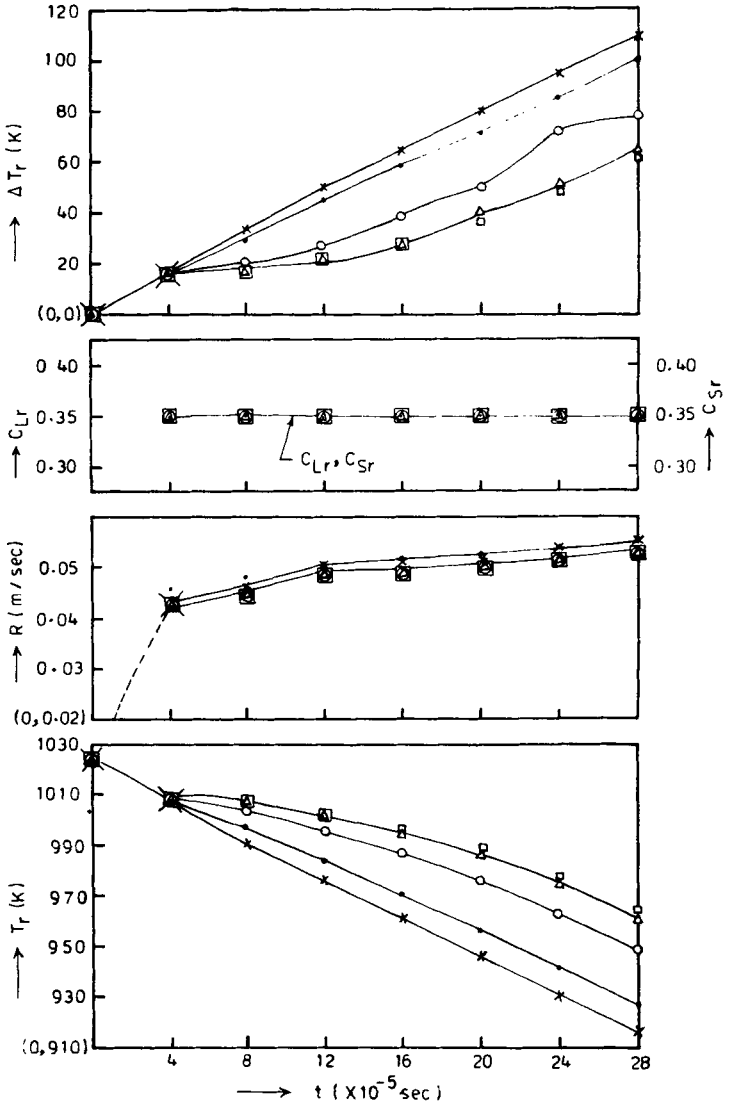

Figure 3. Variation of T_r, R, C_{Lr}, C_{Sr} and ΔT_r with time at (1) $y = 0$ (∗–∗–∗), (2) $y = g$ (●–●–●), (3) $y = 4g$ (o–o–o), (4) $y = 7g$ (△-△-△), (5) $y = 10g$ (□-□-□) for a system with $C_{L0} = 0{\cdot}35$, $T_1 = 1025\,\mathrm{K}$, $\Omega_L = 2{\cdot}8 \times 10^{-21}\,\mathrm{J/atom}$, $\Omega_S = 2{\cdot}8 \times 10^{-20}\,\mathrm{J/atom}$.

effect of external fields can be written as [9, 10]

$$\frac{\partial T}{\partial t}(x,y,t) = D_{TC}\nabla^2 C_L(x,y,t) + D_T\nabla^2 T(x,y,t) + \mathbf{R}\cdot\nabla T(x,y,t) + \mathrm{div}F_T + \mathrm{div}E_T + \frac{\wedge\mathbf{R}}{C_v\rho}\delta(\mathbf{x} - \mathbf{X}_r(y,t)) \quad (1)$$

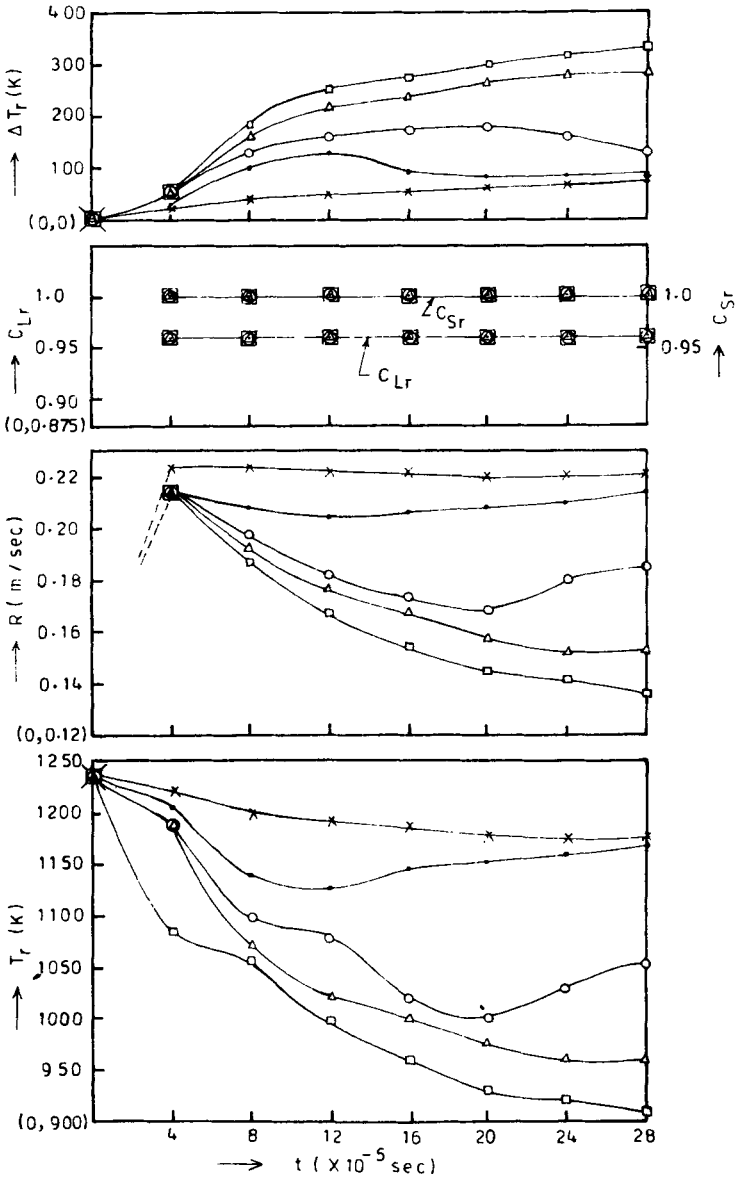

Figure 4. Variation of T_r, R, C_{Lr}, C_{Sr} and ΔT_r with time at (1) $y = 0$ (∗–∗–∗), (2) $y = g$ (•–•–•), (3) $y = 4g$ (o–o–o), (4) $y = 7g$ (△-△-△), (5) $y = 10g$ (□-□-□) for a system with $C_{L0} = 0{\cdot}98$, $T_1 = 1240\,\mathrm{K}$, $\Omega_L = 2{\cdot}8 \times 10^{-21}\,\mathrm{J/atom}$, $\Omega_s = 2{\cdot}8 \times 10^{-20}\,\mathrm{J/atom}$.

and

$$\frac{\partial C_L(x,y,t)}{\partial t} = D_C \nabla^2 C_L(x,y,t) + D_{CT} \nabla^2 T(x,y,t) + \mathbf{R} \cdot \nabla C_L(x,y,t) + \mathrm{div} F_C + \mathrm{div} E_C + (C_{Sr} - C_{Lr}) \mathbf{R} \delta(\mathbf{x} - \mathbf{X}_r(y,t)), \quad (2)$$

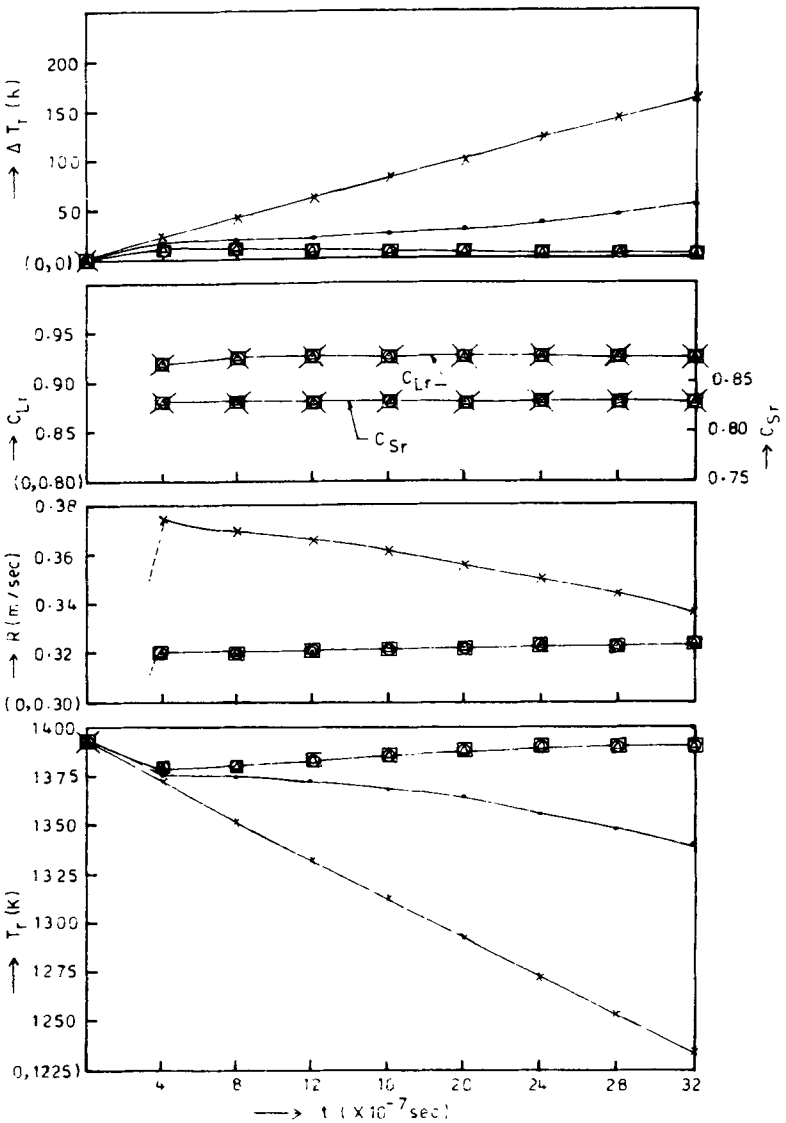

Figure 5. Variation of T_r. R, C_{Lr}, C_{Sr} and ΔT_r with time at (1) $y = 0$ (*–*–*), (2) $y = g$ (•–•–•), (3) $y = 4g$ (o–o–o), (4) $y = 7g$ (Δ-Δ-Δ), (5) $y = 10g$ (□-□-□) for a system with $C_{L0} = 0{\cdot}9$, $T_1 = 1393\,\text{K}$, $\Omega_L = 2{\cdot}8 \times 10^{-19}\,\text{J/atom}$, $\Omega_S = 2{\cdot}8 \times 10^{-20}\,\text{J/atom}$.

where C_L is the relative concentration of B atoms in A–B system, T is the temperature of the melt, D_T is the diffusivity, C_v is the volume specific heat and ρ is the density of the solid volume. D_C is the diffusion coefficient, D_{CT} and D_{TC} are related to the Onsager's coefficients due to interdependence of mass and heat flow, R is the rate of growth of the solid phase, x is the direction of growth and y is the coordinate perpendicular to it, t is the time coordinate, E_T and E_C are the heat and mass flux controlled by external fields,

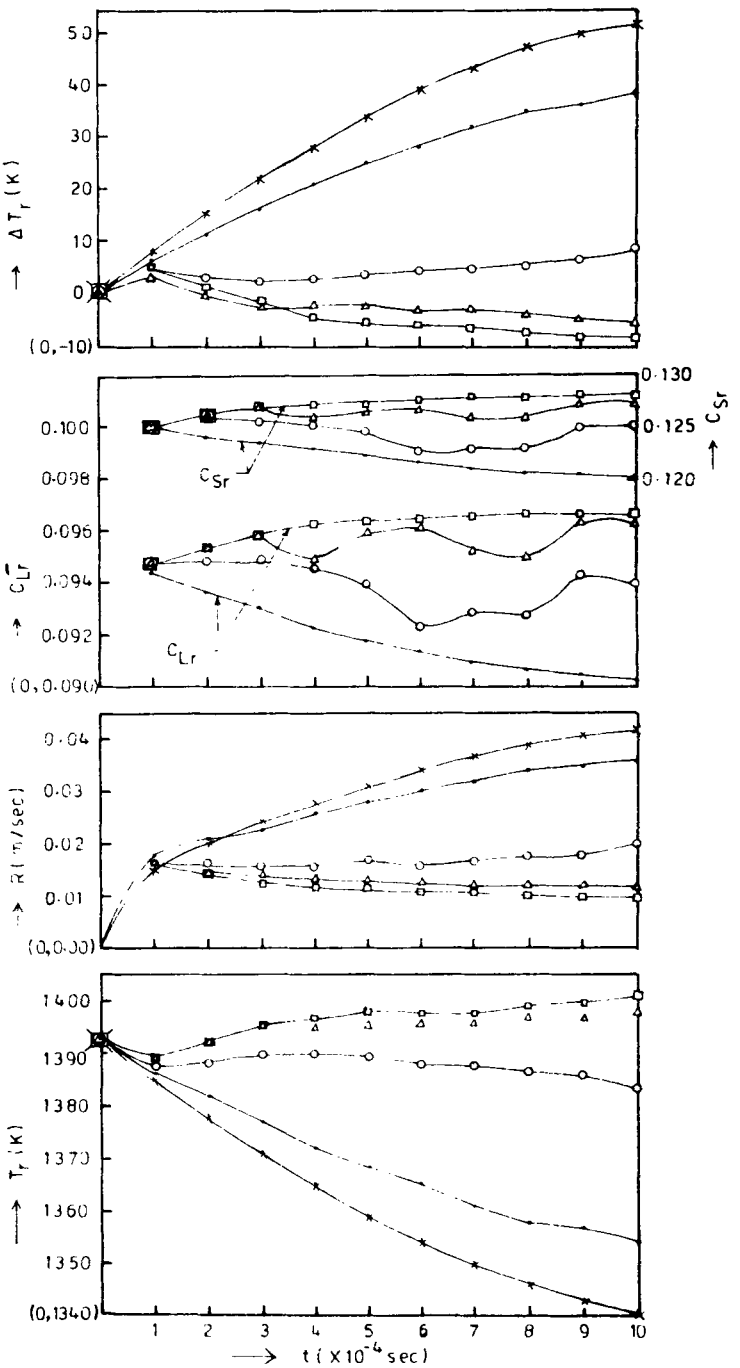

Figure 6. Variation of T_r, R, C_{Lr}, C_{Sr} and ΔT_r with time at (1) $y = 0$ (*–*–*), (2) $y = g$ (•–•–•), (3) $y = 4g$ (o–o–o), (4) $y = 7g$ (△-△-△), (5) $y = 10g$ (□-□-□) for system with $C_{L0} = 0{\cdot}9$, $T_1 = 1698\,\text{K}$, $\Omega_L = -2{\cdot}33 \times 10^{-20}\,\text{J/atom}$, $\Omega_S = -2{\cdot}47 \times 10^{-20}\,\text{J/atom}$.

respectively, F_T and F_C are the stochastic terms that represent the flux of heat and mass due to fluctuations, C_{Sr} and C_{Lr} are the solid and liquid concentrations at the interface $\mathbf{X}_r(t)$, respectively, $\wedge$ is the latent heat per unit volume.

For evaluation of the fluctuation terms F_T and F_C, the Langevin method of stochastic differential equations has been used [7, 9, 11]. According to this method the average of the random fluctuations can be written as

$$\langle \text{div}\, F_T \rangle = \langle \text{div}\, F_C \rangle = 0$$

which is the characteristic of a Markov process. The position of the solid–liquid interface

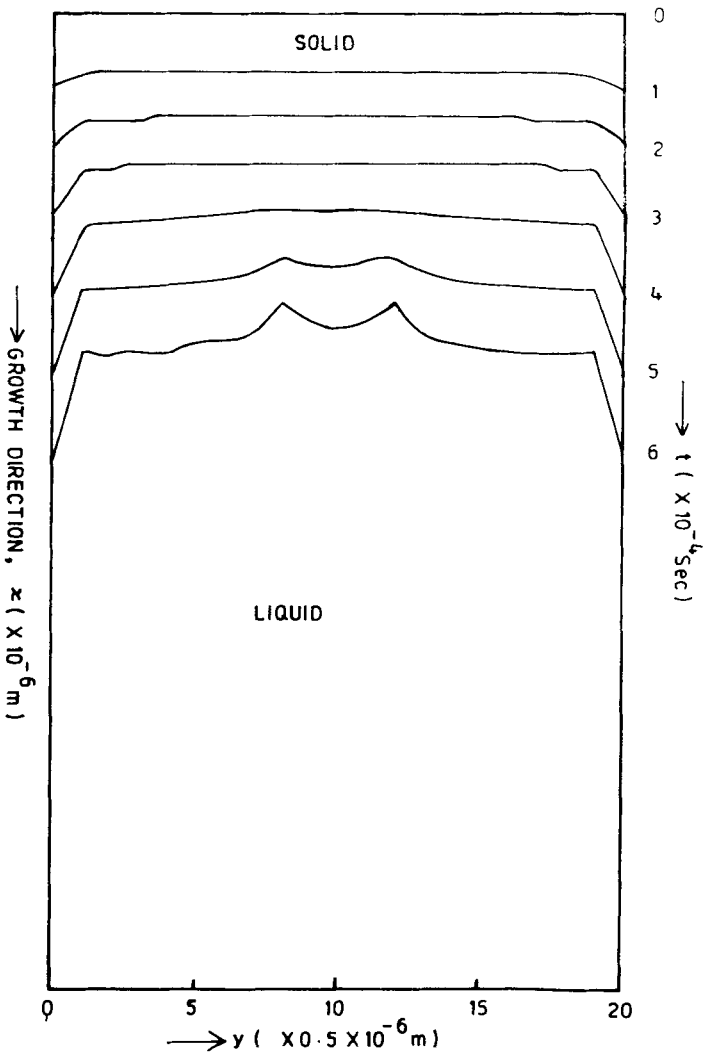

Figure 7a. Time evolution of the solid–liquid interface for a system with $C_{L0} = 0{\cdot}3$, $T_1 = 1503\,\text{K}$, $\Omega_L = 2{\cdot}8 \times 10^{-20}\,\text{J/atom}$, $\Omega_S = 2{\cdot}33 \times 10^{-20}\,\text{J/atom}$.

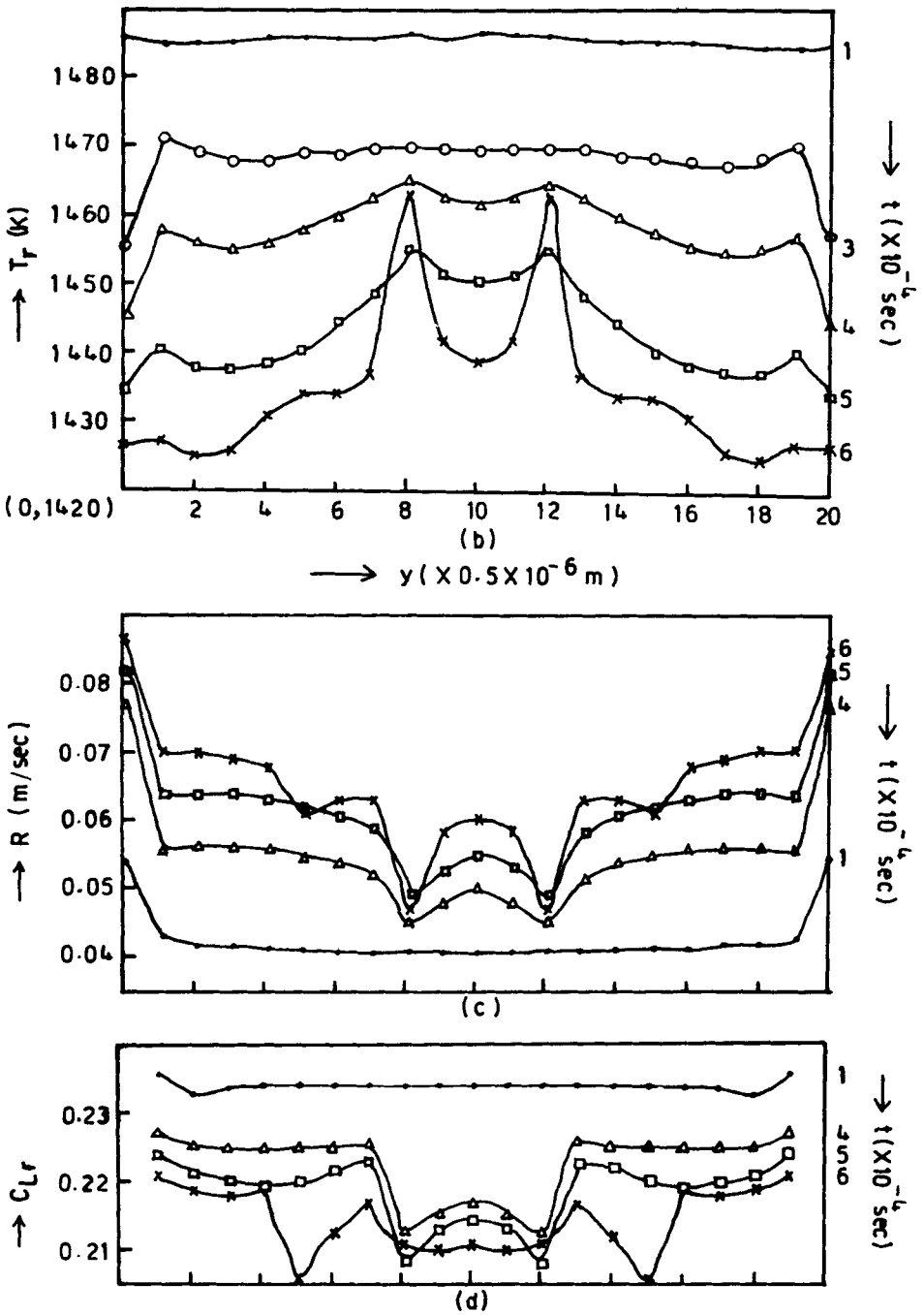
1480
1470
1460
1450
1440
1430
T_r (K)
(0,1420)
2
4
6
8
10
12
14
16
18
20
(b)
y (X 0·5 X 10^{-6} m)
t (X 10^{-4} sec)
1
3
4
5
6
0·08
0·07
0·06
0·05
0·04
R (m/sec)
(c)
0·23
0·22
0·21
C_{Lr}
(d)

Figures 7(b–d).

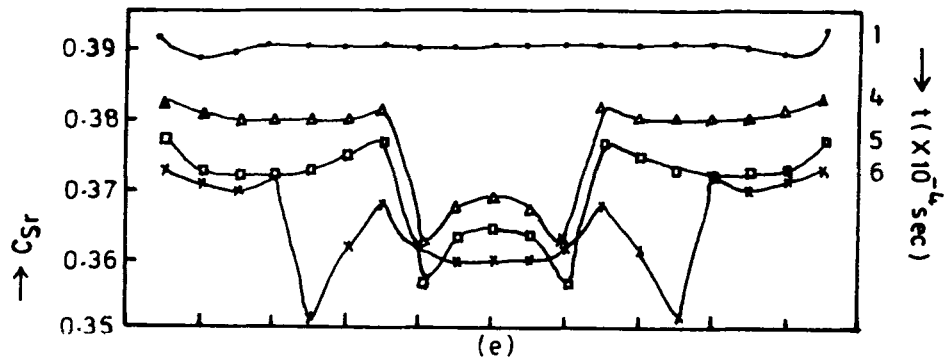

Figures 7(b–e). Time evolution of the interface: **(b)** temperature, **(c)** rate of growth, **(d)** concentration of the liquid phase, **(e)** concentration of the solid phase for a system with $C_{L0} = 0{\cdot}3$, $T_I = 1503\,\mathrm{K}$, $\Omega_L = 2{\cdot}8 \times 10^{-20}\,\mathrm{J/atom}$, $\Omega_S = 2{\cdot}33 \times 10^{-20}\,\mathrm{J/atom}$.

is given by

$$\mathbf{X}_r(t) = \mathbf{n}_r \int_{t_0}^{t} R(t')\mathrm{d}t' + \mathbf{X}_r(t_0), \tag{3}$$

where $\mathbf{n}_r$ is normal to the interface and $\mathbf{X}_r(t_0)$ is its initial position.

The kinetic processes at the solid–liquid interface have been modeled using a microscopic description of the process of solidification i.e., by assigning probabilities to individual atoms as they make transition from a liquid-like configuration to a solid-like configuration and then averaging over the corresponding phases to determine the probability of formation of the new phase. The probability of creation of new monoatomic layer of the solid phase with concentration C'_{Sr} per unit time can be written as [8, 9]

$$P_0(C_{Sr}, C'_{Sr}, t) = P^{B}_{\rho\Delta\times C_{Sr}} P^{A}_{\rho\Delta\times(1-C_{Sr})}, \tag{4}$$

where

$$P^{A,B}_{m_{A,B}} = \binom{N^S_{A,B}}{m_{A,B}} (P^{A,B}_B)^{(m_{A,B})} (1 - P^{A,B}_B)^{(N^S_{A,B} - m_{A,B})},$$

$$N^S_A = \nu^L_A (1 - C_{Lr})\rho^L,$$

$$N^S_B = \nu^L_B C_{Lr}\rho^L,$$

$$m_A = \overline{(1 - C_{Sr})\rho^S(y)\Delta x} = N^S_A P^A_3,$$

$$m_B = \overline{C_{Sr}\rho^S(y)\Delta x} = N^S_B P^B_3,$$

$$P^A_3 = P^A_1 F_A(T_r(x,y,t), C_{Lr}(x,y,t), C_{Sr}(x,y,t)),$$

$$P^B_3 = P^B_1 F_B(T_r(x,y,t), C_{Lr}(x,y,t), C_{Sr}(x,y,t)),$$

$$P^A_1 = \exp(-U_A/K_B T_r),$$

$$P^B_1 = \exp(-U_B/K_B T_r),$$

$$F_A = \left[1 - \exp\left(-\frac{\Delta\mu_A}{K_B T_r}\right)\right],$$

$$F_B = \left[1 - \exp\left(-\frac{\Delta\mu_B}{K_B T_r}\right)\right].$$

$\Delta\mu_{A,B}$ is the change in chemical potential per A,B atom transfer from the solid to the liquid phase, K_B is the Boltzmann constant, T_r is the interface temperature, $P_3^{A,B}$ is the probability of one A,B atom joining the solid phase per unit time, $P_1^{A,B}$ is the probability of one A,B atom transition from liquid to solid phase, $U_{A,B}$ is the activation

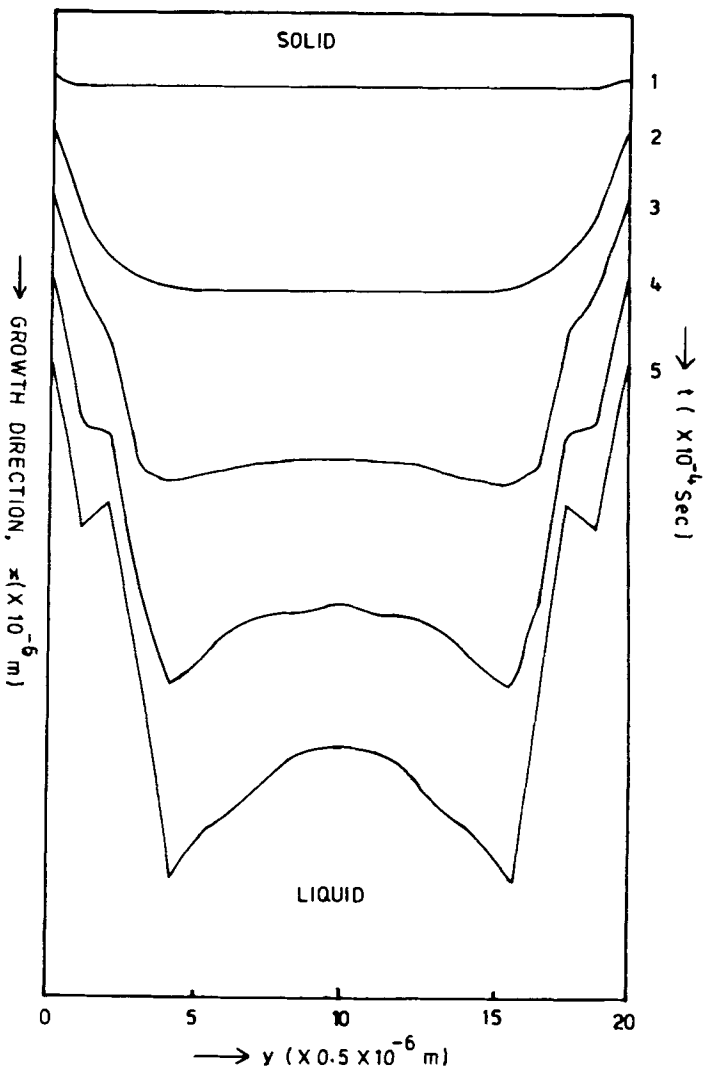

Figure 8(a). Time evolution of the solid–liquid interface for a system with $C_{L0} = 0{\cdot}7$, $T_1 = 1643$ K, $\Omega_L = 2{\cdot}8 \times 10^{-20}$ J/atom, $\Omega_S = 2{\cdot}33 \times 10^{-20}$ J/atom.

energy of transition of one A,B atom from liquid to solid phase across the interface, $\rho^{L,S}$ is the total number of atoms per unit volume in a monoatomic layer at the interface in the liquid, solid phase, Δx is the thickness of the solid grown, m_A and m_B are respectively the number of A and B component that cross the interface from liquid to solid phase per unit area in the time interval Δt, $N^S_{A,B}$ is the number of possible transitions of one A,B atom from the liquid to the solid phase across the interface per unit time and $\nu^L_{A,B}$ is the frequency of thermal vibrations of the atoms of A,B component in the liquid phase.

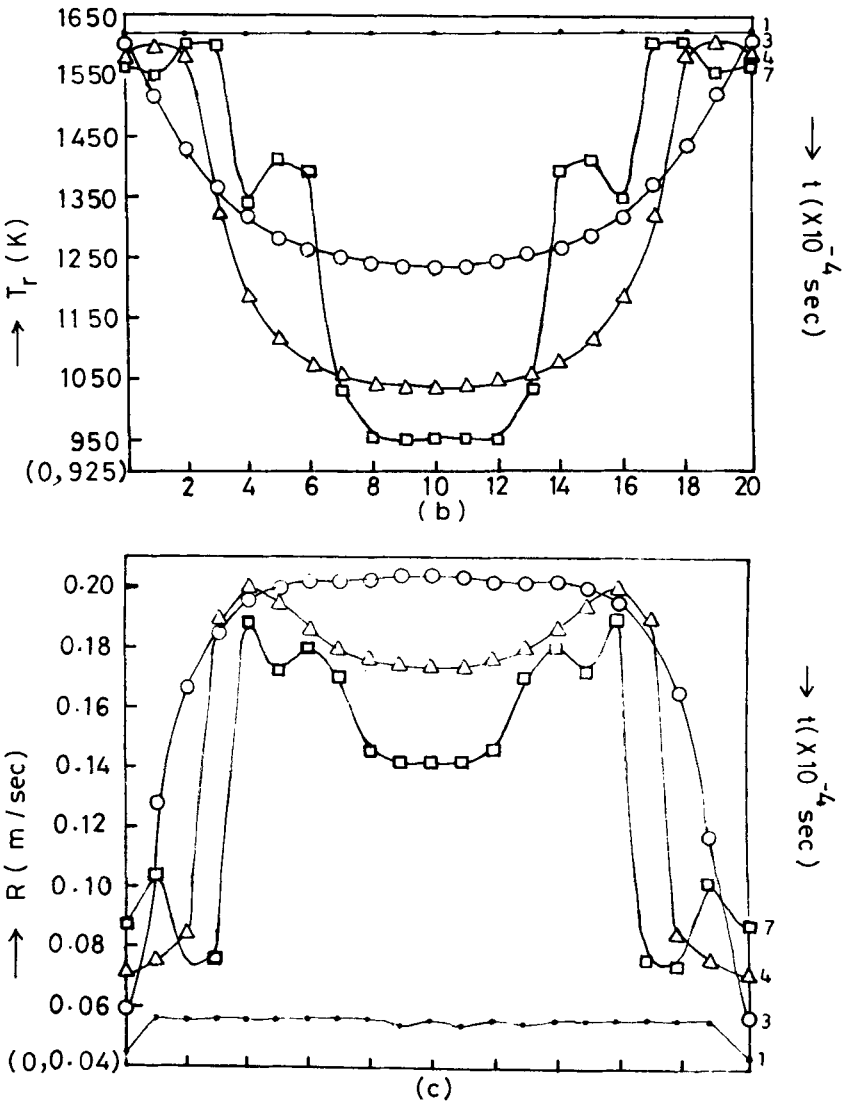

Figures 8(b, c).

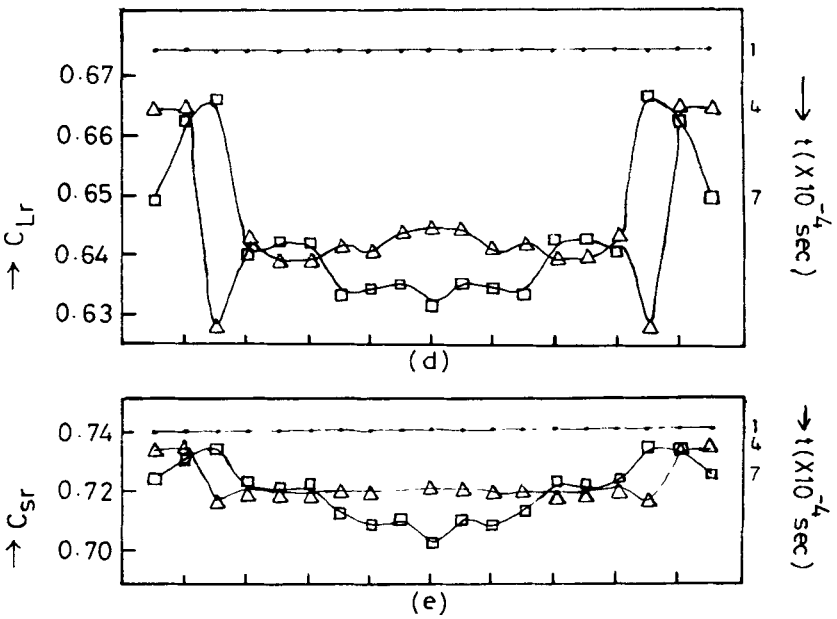

Figures 8(b–e). Time evolution of the interface: **(b)** temperature, **(c)** rate of growth, **(d)** concentration of the liquid phase, **(e)** concentration of the solid phase for a system with $C_{L0} = 0{\cdot}7$, $T_i = 1643\,\text{K}$, $\Omega_L = 2{\cdot}8 \times 10^{-20}\,\text{J/atom}$, $\Omega_S = 2{\cdot}33 \times 10^{-20}\,\text{J/atom}$.

The average concentration and rate of growth of the solid phase have been evaluated by using the probability of formation of a new monoatomic layer and are given by [9]

$$\overline{C}_{Sr}(x,y,t) = \frac{C_{Lr}F_B(T_r, C_{Lr}, C_{Sr})}{C_{Lr}F_B(T_r, C_{Lr}, C_{Sr}) + (1 - C_{Lr})F_A(T_r, C_{Lr}, C_{Sr})} \tag{5}$$

and

$$\overline{R}(x,y,t) = a_0 \nu P_1^B [C_{Lr}F_B(T_r, C_{Lr}, C_{Sr}) + (1 - C_{Lr})F_A(T_r, C_{Lr}, C_{Sr})], \tag{6}$$

where a_0 is the lattice constant of the solid. The change in chemical potential per A,B atom transfer from solid to liquid phase, $\Delta\mu_{A,B}$, for the non ideal solutions taking into account the interaction effects of the constituents of the binary alloy are given by [9]

$$\Delta\mu_A = \frac{\Delta H_A(T_A - T_r)}{T_A} + K_B T_r \ln\frac{(1 - C_{Lr})}{(1 - C_{Sr})} + \Omega_L(C_{Lr})^2 - \Omega_S(C_{Sr})^2 \tag{7}$$

and

$$\Delta\mu_B = \frac{\Delta H_B(T_B - T_r)}{T_B} + K_B T_r \ln\frac{C_{Lr}}{C_{Sr}} + \Omega_L(1 - C_{Lr})^2 - \Omega_S(1 - C_{Sr})^2, \tag{8}$$

where $\Delta H_{A,B}$ is the enthalpy of fusion of A,B component at its melting temperature $T_{A,B}$ [2].

The coupled equations (1), (2), (3), (5) and (6) can be solved to obtain the time evolution of temperature, concentration of the liquid phase, interface shape, concentration of the solid phase and rate of growth respectively.

Finite difference method alongwith successive over-relaxation method has been used to solve these equations. The boundary conditions chosen correspond to crystal pulling technique of crystal growth. The details of the numerical scheme alongwith the boundary conditions are given in ref. [9, 10]. Calculations were performed to obtain time evolution of temperature, concentrations of the liquid and solid phase, rate of growth of the solid phase and evolution of the solid–liquid interface shape. The representative systems

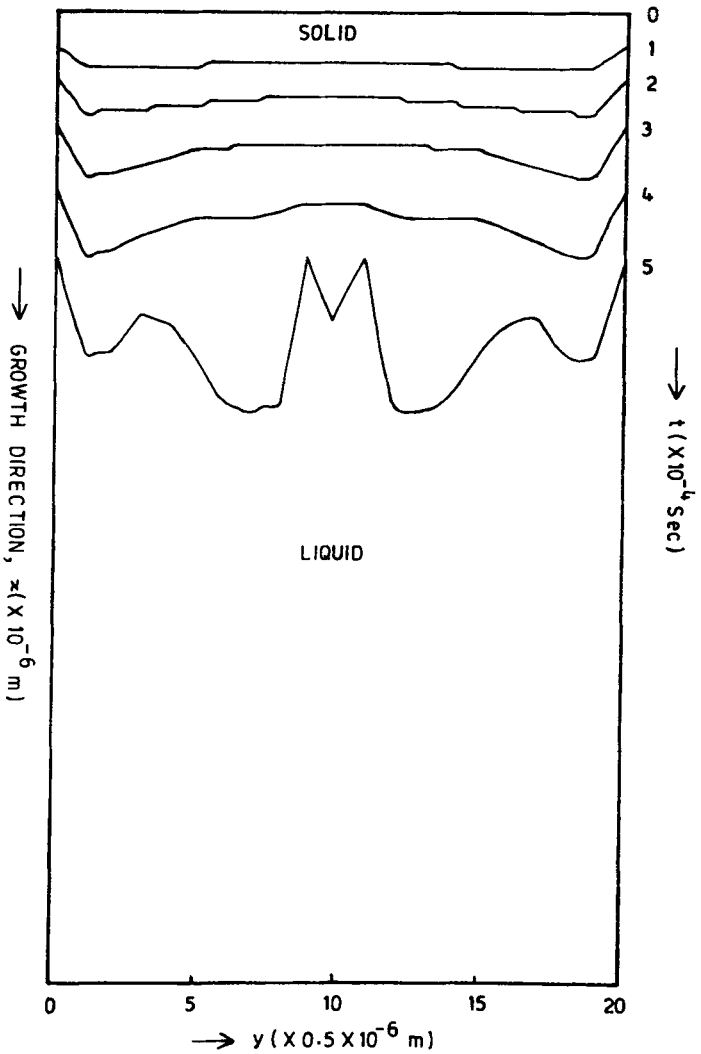

Figure 9a. Time evolution of the solid–liquid interface for a system with $C_{L0} = 0{\cdot}9$, $T_1 = 1703$ K, $\Omega_L = 2{\cdot}8 \times 10^{-20}$ J/atom, $\Omega_S = 2{\cdot}33 \times 10^{-20}$ J/atom.

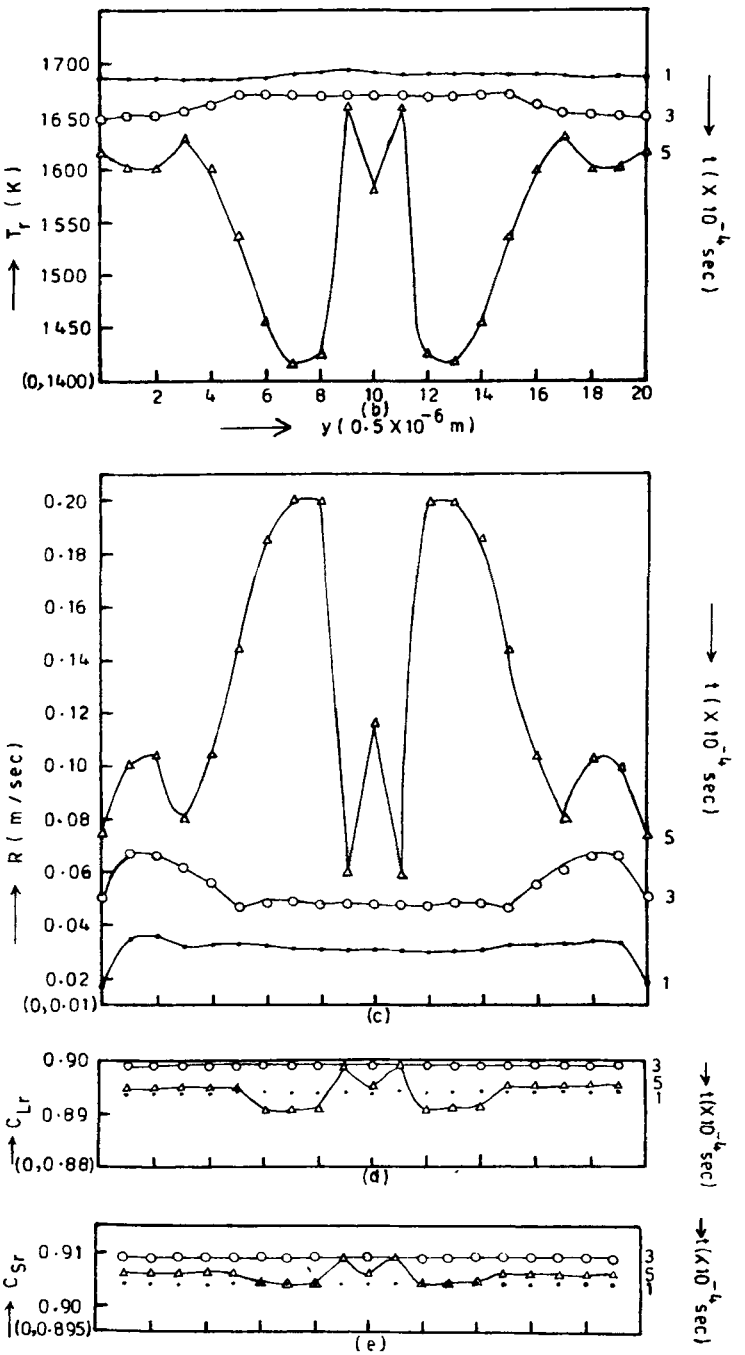

Figures 9(b–e). Time evolution of the interface: (**b**) temperature, (**c**) rate of growth, (**d**) concentration of the liquid phase, (**e**) concentration of the solid phase for a system with $C_{L0} = 0{\cdot}9$, $T_I = 1703\,\mathrm{K}$, $\Omega_L = 2{\cdot}8 \times 10^{-20}\,\mathrm{J/atom}$, $\Omega_S = 2{\cdot}33 \times 10^{-20}\,\mathrm{J/atom}$.

selected for study are

System I	$\Omega_L = 2{\cdot}8 \times 10^{-20}$ J/atom	$\Omega_S = 2{\cdot}33 \times 10^{-20}$ J/atom
System II	$\Omega_L = 2{\cdot}8 \times 10^{-21}$ J/atom	$\Omega_S = 2{\cdot}8 \times 10^{-20}$ J/atom
System III	$\Omega_L = 2{\cdot}8 \times 10^{-19}$ J/atom	$\Omega_S = 2{\cdot}8 \times 10^{-20}$ J/atom
System IV	$\Omega_L = -2{\cdot}33 \times 10^{-20}$ J/atom	$\Omega_S = -2{\cdot}47 \times 10^{-20}$ J/atom
System V	$\Omega_L = -2{\cdot}8 \times 10^{-20}$ J/atom	$\Omega_S = -2{\cdot}8 \times 10^{-19}$ J/atom
System VI	$\Omega_L = -2{\cdot}8 \times 10^{-20}$ J/atom	$\Omega_S = -2{\cdot}8 \times 10^{-21}$ J/atom

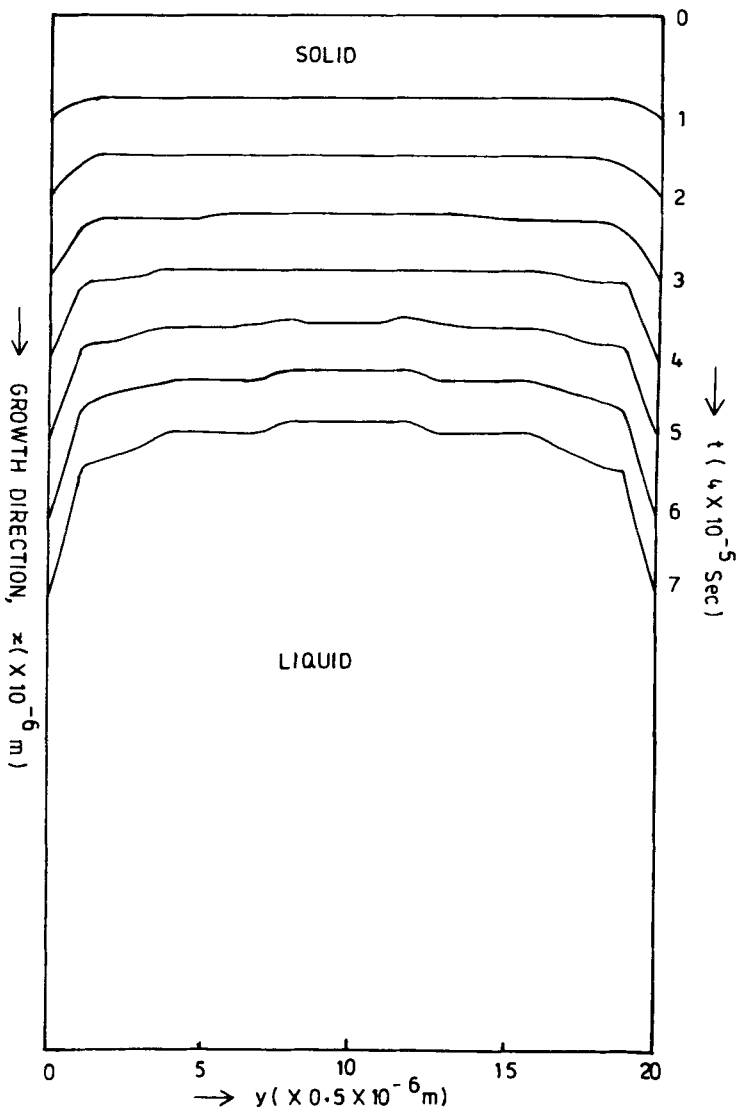

Figure 10a. Time evolution of the solid–liquid interface for a system with $C_{L0} = 0{\cdot}9$, $T_1 = 1200$ K, $\Omega_L = 2{\cdot}8 \times 10^{-21}$ J/atom, $\Omega_S = 2{\cdot}8 \times 10^{-20}$ J/atom.

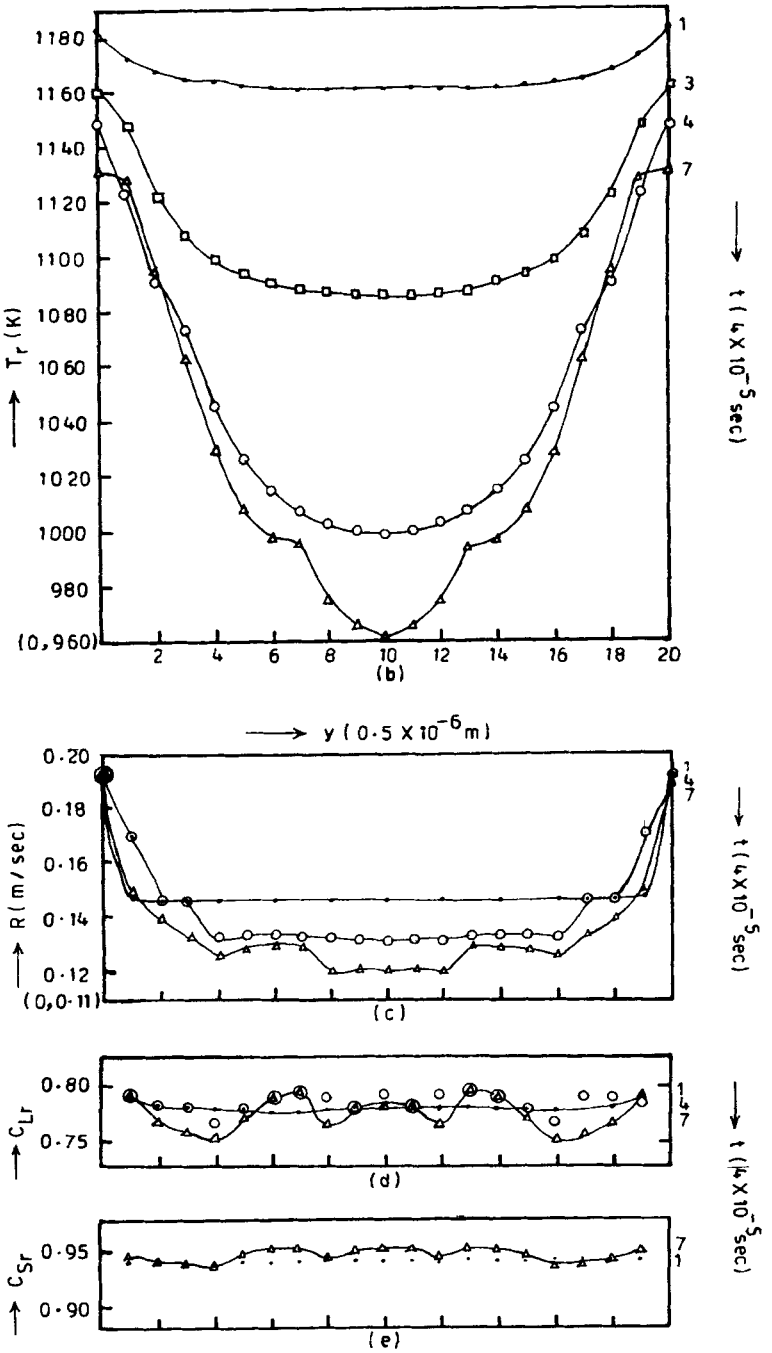

Figures 10(b–e). Time evolution of the interface: (**b**) temperature, (**c**) rate of growth, (**d**) concentration of the liquid phase, (**e**) concentration of the solid phase for a system with $C_{L0} = 0{\cdot}9$, $T_1 = 1200\,\text{K}$, $\Omega_L = 2{\cdot}8 \times 10^{-21}\,\text{J/atom}$, $\Omega_S = 2{\cdot}8 \times 10^{-20}\,\text{J/atom}$.

3. Results and discussion

3.1 *Time evolution of interface temperature T_r, concentrations C_{Lr} and C_{Sr}, rate of growth R and undercooling ΔT_r at various points along the interface*

The time evolution of interface temperature T_r, concentrations C_{Lr} and C_{Sr}, rate of growth R and undercooling $\Delta T_r(T_1 - T_r)$ for all the six systems mentioned above is shown in figures 1–6. These figures show the time dependence at edge (point '0' i.e., point next to the wall of the container), the centre of the specimen ($10g$) and at three other points ($g, 4g, 7g$) between edge and the centre, along the interface (viz. the y direction).

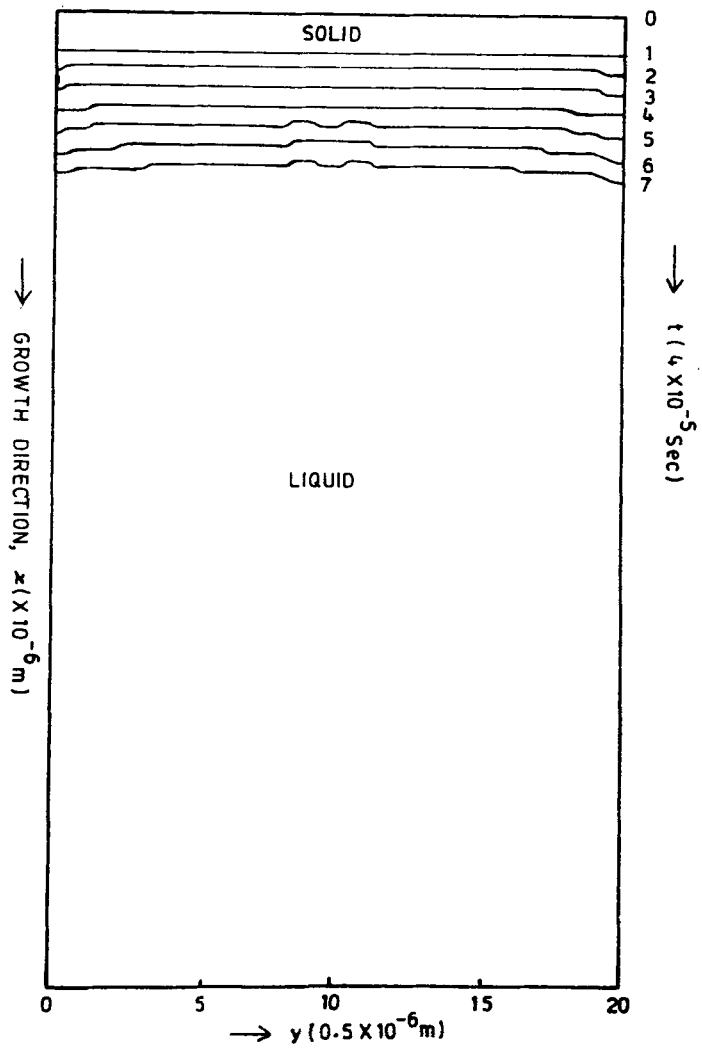

Figure 11(a). Time evolution of the solid–liquid interface for a system with $C_{L0} = 0{\cdot}25$, T_1=1050 K, $\Omega_L = 2{\cdot}8 \times 10^{-21}$ J/atom, $\Omega_S = 2{\cdot}8 \times 10^{-20}$ J/atom.

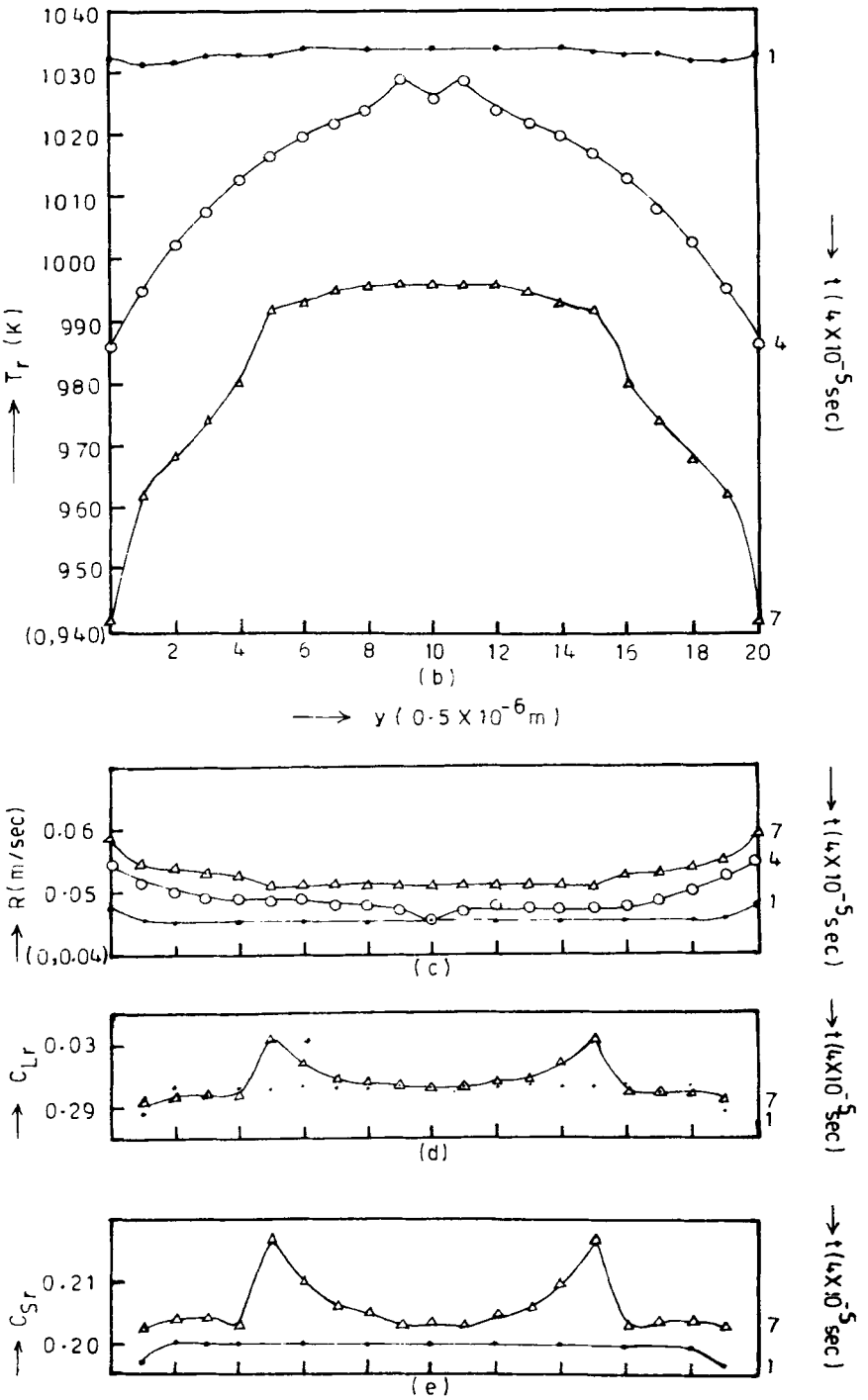

Figures 11(b–e). Time evolution of the interface: (**b**) temperature, (**c**) rate of growth, (**d**) concentration of the liquid phase, (**e**) concentration of the solid phase for a system with $C_{L0} = 0{\cdot}25$, T_1=1050 K, $\Omega_L = 2{\cdot}8 \times 10^{-21}$ J/atom, $\Omega_S = 2{\cdot}8 \times 10^{-20}$ J/atom.

g is the meshwidth in y direction. As the results are symmetric about an axis passing through the middle of the specimen parallel to the direction of growth (i.e. x-axis), observations only up to the centre point ($10g$) are given. Some typical results are discussed below.

System I. From figure 1 it is observed that the temperature of the interface at the edge decreases nonlinearly with time, rate of growth increases nonlinearly and shows a tendency to become constant. Both solid and liquid concentrations decrease below the equilibrium value and attain a constant difference $(C_{Sr} - C_{Lr})$ in time and the undercooling increases with time nonlinearly.

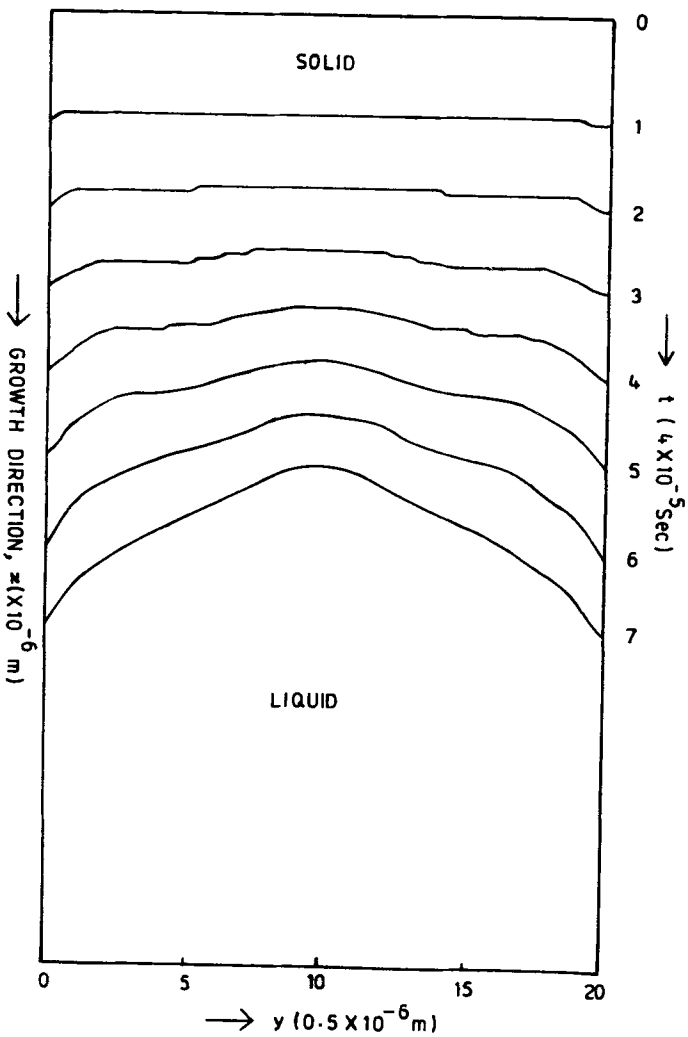

Figure 12(a). Time evolution of the solid–liquid interface for a system with $C_{L0} = 0{\cdot}98$, $T_1 = 1240\,\text{K}$, $\Omega_L = 2{\cdot}8 \times 10^{-21}\,\text{J/atom}$, $\Omega_S = 2{\cdot}8 \times 10^{-20}\,\text{J/atom}$.

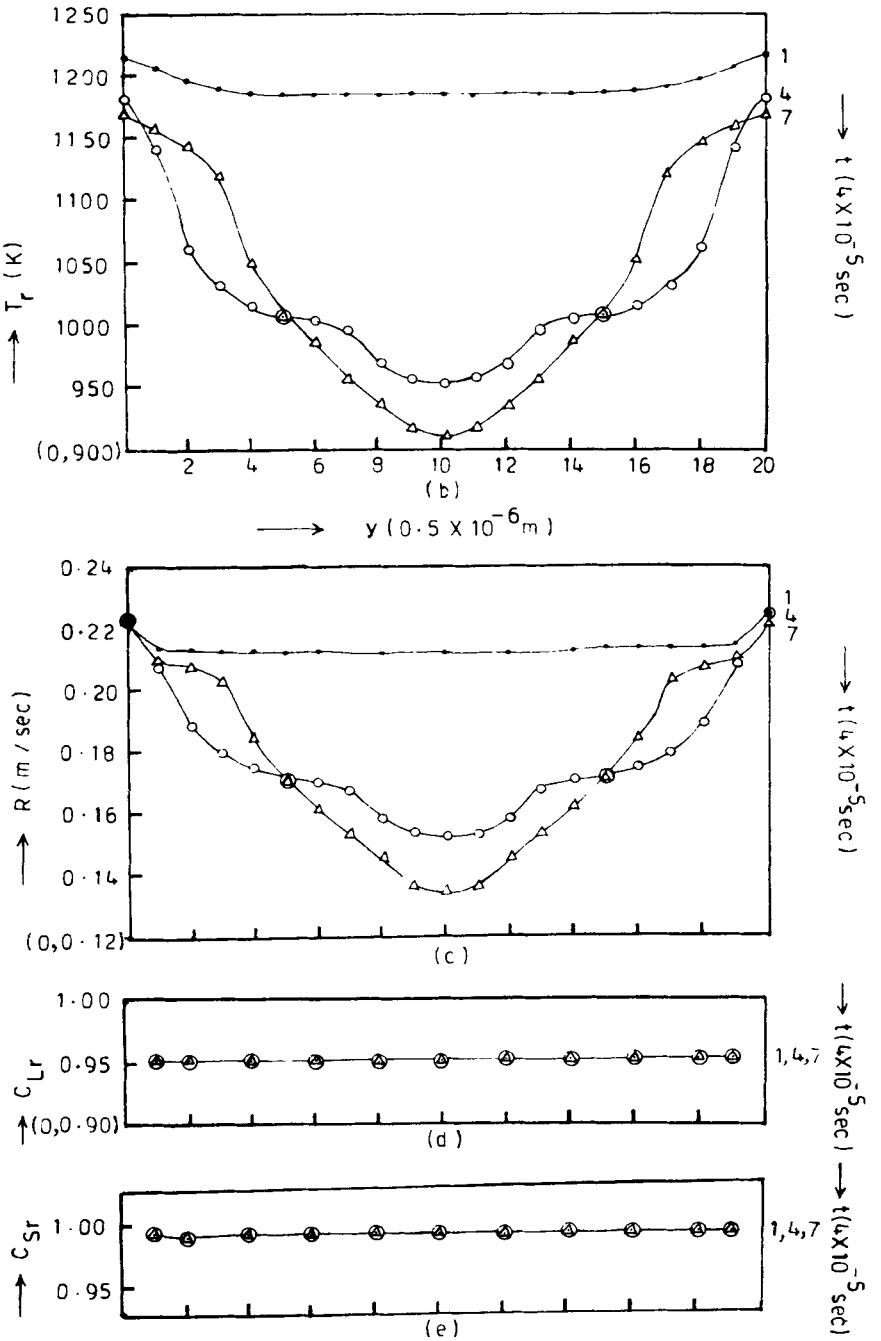

Figures 12(b–e). Time evolution of the interface: **(b)** temperature, **(c)** rate of growth, **(d)** concentration of the liquid phase, **(e)** concentration of the solid phase for a system with $C_{L0} = 0{\cdot}98$, $T_1 = 1240\,\text{K}$, $\Omega_L = 2{\cdot}8 \times 10^{-21}\,\text{J/atom}$, $\Omega_S = 2{\cdot}8 \times 10^{-20}\,\text{J/atom}$.

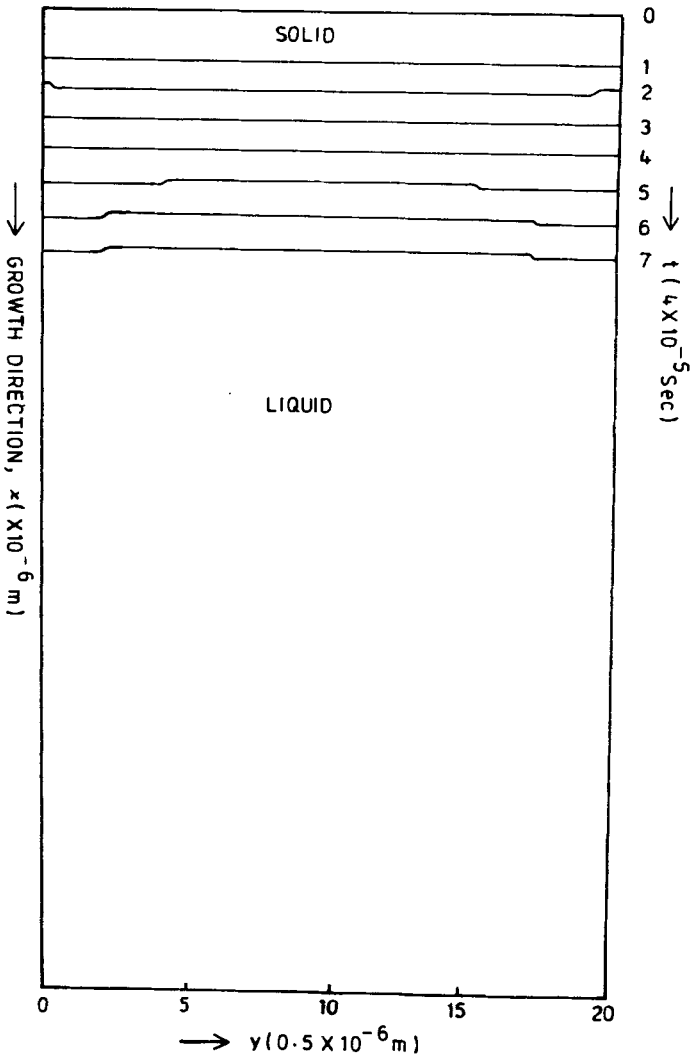

Figure 13(a). Time evolution of the solid–liquid interface for a system with $C_{L0} = 0{\cdot}02$, $T_1 = 1190\,\text{K}$, $\Omega_L = 2{\cdot}8 \times 10^{-21}\,\text{J/atom}$, $\Omega_S = 2{\cdot}8 \times 10^{-20}\,\text{J/atom}$.

Moving inside from the edge along the interface, the interface temperature goes on increasing and the interface is less undercooled at the inside points with minimum of undercooling occurring at the centre. The rate of growth as well as the concentrations of the liquid and solid phase decreases along the interface towards the centre.

These plots show the effect of cooling the sample equally from the boundaries while an exponential external temperature gradient is maintained in the growth direction. The effect of cooling reaches the centre of the sample some time later.

The plots shown in figure 2 show different characteristics than that shown in figure 1. Here the temperature at the edge of the interface decreases linearly, at a distance g it fluctuates about a decreasing trend, at distance $4g$ and $7g$ it decreases exponentially

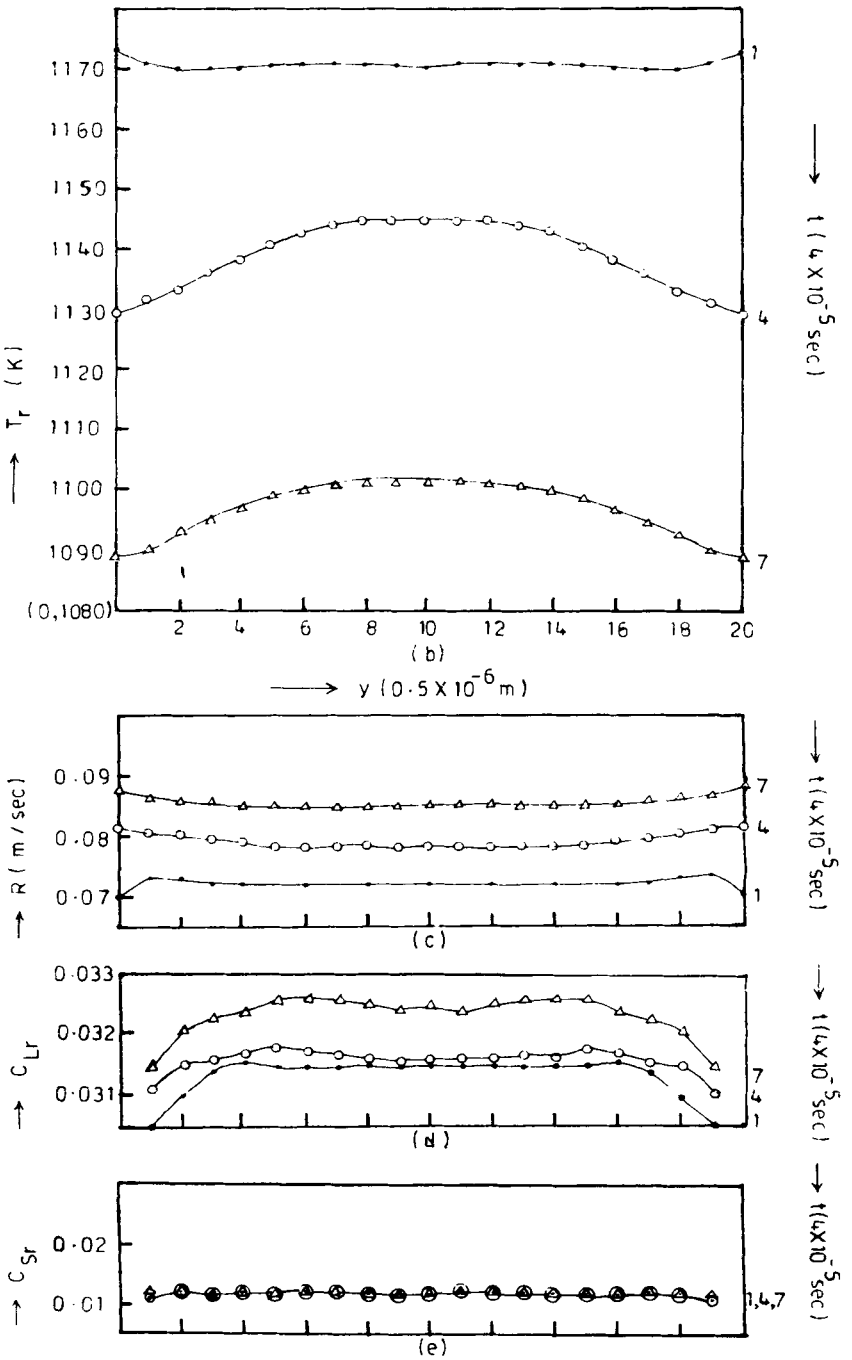

Figures 13(b–e). Time evolution of the interface: **(b)** temperature, **(c)** rate of growth, **(d)** concentration of the liquid phase, **(e)** concentration of the solid phase for a system with $C_{L0} = 0{\cdot}02$, $T_1 = 1190\,\text{K}$, $\Omega_L = 2{\cdot}8 \times 10^{-21}\,\text{J/atom}$, $\Omega_S = 2{\cdot}8 \times 10^{-20}\,\text{J/atom}$.

and then increases nonlinearly and at the centre there is an exponential decrease of temperature with time. A reverse behaviour can be seen in the rate of growth and undercooling plots. Both C_{Lr} and C_{Sr} decreases with time and attains constant values.

A relative analysis of the plots for this system shows that the fluctuations mentioned above are observed only when the average liquid concentration C_{L0} is equal to or greater than 0·5. Also the rate of growth is maximum when $C_{L0} = 0{\cdot}9$, and minimum at $C_{L0} = 0{\cdot}2$, which shows dependence of rate of growth on concentration C_{L0}.

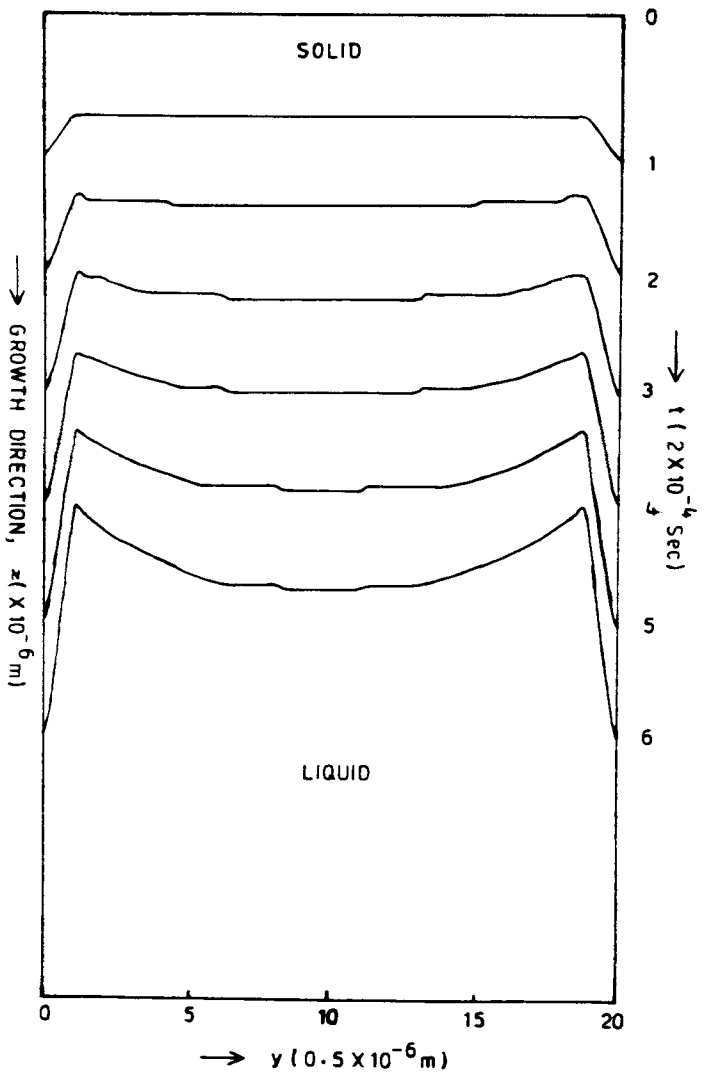

Figure 14(a). Time evolution of the solid–liquid interface for a system with $C_{L0} = 0{\cdot}5$, $T_1 = 1065\,\text{K}$, $\Omega_L = 2{\cdot}8 \times 10^{-21}\,\text{J/atom}$, $\Omega_S = 2{\cdot}8 \times 10^{-20}\,\text{J/atom}$.

System II. A linear decrease in temperature of the various points of interface with time can be seen in figure 3. Temperature increases gradually along the interface towards the centre of the sample. The rate of growth varies nonlinerly with time and shows a tendency to achieve steady state growth conditions. Also, it is maximum at the edge and minimum at the centre of the sample. The solid and the liquid concentrations are practically

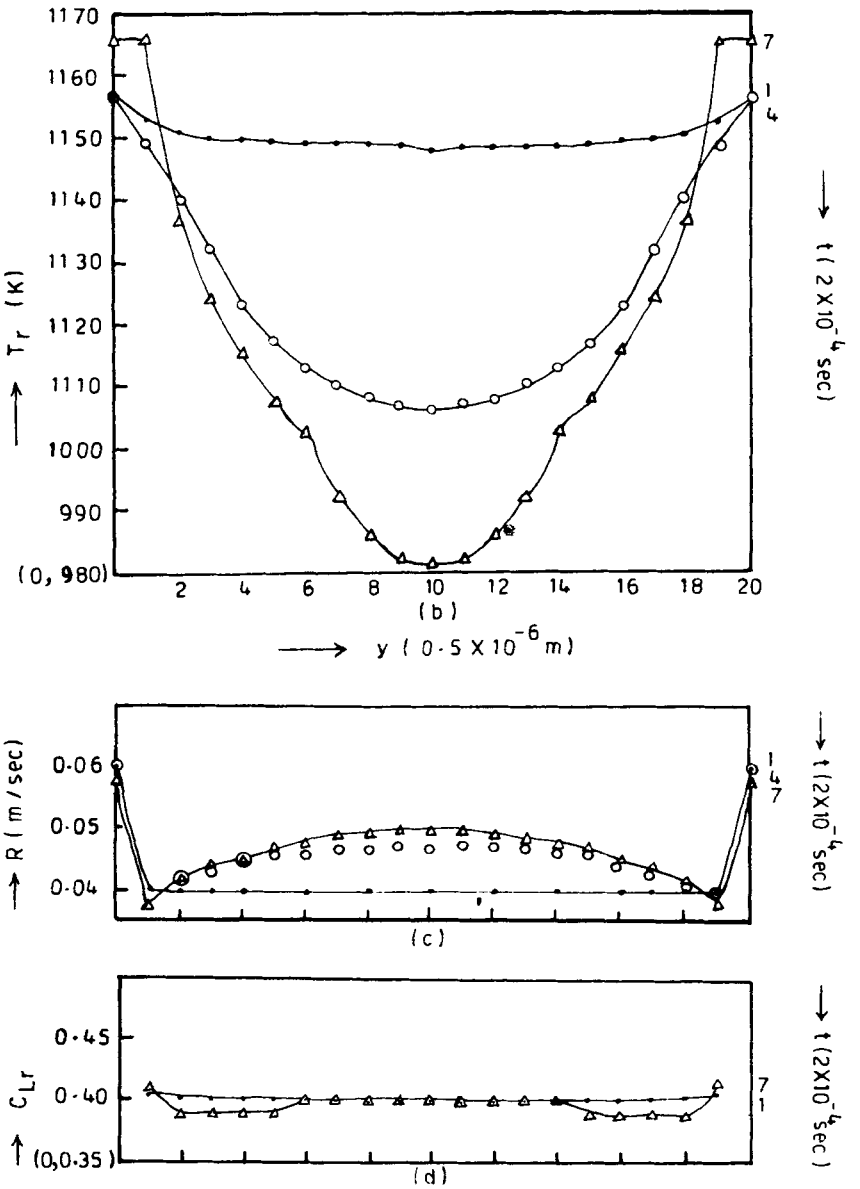

Figures 14(b–d).

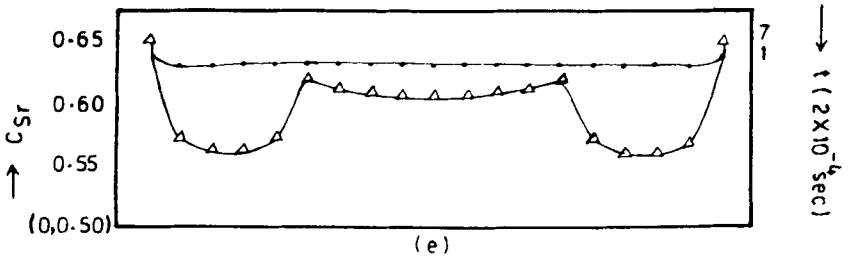

Figures 14(b–e). Time evolution of the interface: (**b**) temperature, (**c**) rate of growth, (**d**) concentration of the liquid phase, (**e**) concentration of the solid phase for a system with $C_{L0} = 0{\cdot}5$, $T_1 = 1065$ K, $\Omega_L = 2{\cdot}8 \times 10^{-21}$ J/atom, $\Omega_S = 2{\cdot}8 \times 10^{-20}$ J/atom.

constant with time, which means the ratio C_{Sr}/C_{Lr} (the so called segregation coefficient) is fixed.

For this system at $C_{L0} = 0{\cdot}35$ the congruent melting takes place (both C_{Lr} and $C_{Sr} = 0{\cdot}35$). For $C_{L0} \geq 0{\cdot}5$, fluctuations in C_{Lr} and C_{Sr} can be seen. The extreme case is shown in figure 4 for $C_{L0} = 0{\cdot}98$. The temperature as well as the rate of growth at the centre of the sample is the lowest in this case, i.e. a decrease in rate of growth is observed with a decreasing temperature. Both C_{Lr} and C_{Sr} are constant in time. The decrease in the rate of growth with decreasing temperature shows that it is in the region of the continuous growth where the rate of growth decreases by further increase in undercooling [3].

System III. A linear decrease in interface temperature with time at the edge of the sample can be seen in figure 5. With time the temperature at the centre of the sample at the interface stays approximately close to the equilibrium melting temperature. The rate of growth is very high (0·9 m/s) at $C_{L0} = 0{\cdot}5$ and decreases for $C_{L0} > 0{\cdot}5$ or $C_{L0} < 0{\cdot}5$. With time the rate of growth of the various points at the interface approximately reaches the same value. Both C_{Lr} and C_{Sr} are practically constant. Congruent melting takes place at $C_{L0} = 0{\cdot}5$, where both C_{Lr} and C_{Sr} are equal (i.e. 0·5).

System IV. The behaviour of the plots shown in figure 6 is the same as those of figure 1 for system I except that in the time–temperature plots an increase in temperature above $T_{eq}(= T_1)$ at the centre of the sample is observed.

The plots for system V are similar to plots of system III and the plots for system VI are similar to those of system II.

In all the system only some typical results are given. The trends shown by these plots in all the six systems therefore agree with the experimentally observed results. These plots are also similar to Chvoj's [12] results for single component system and also to one-dimensional binary system [6]. From this study the effect of concentration on rate of growth can be observed.

3.2 *Evolution of the solid–liquid interface shape* $X_r(y)$

In this section the plots of solid–liquid interface shape with time are given alongwith the plots of its temperature, solid and liquid concentrations and rate of growth. In the present

model the solid–liquid interface is chosen to be a flat surface initially. As the solidification proceeds the heat of fusion is evolved at this surface and the solute atoms diffuse away according to the boundary conditions given in § 3.1 of part I. Many interesting shapes of the interface observed are discussed below.

System I. It is seen in figure 7(a) that the interface remains smooth up to two time steps and becomes progressively curved with kinks at points $8g$ and $12g$. The temperature–time plots, given in figure 7(b) show large heating of these points. The rate of growth is the

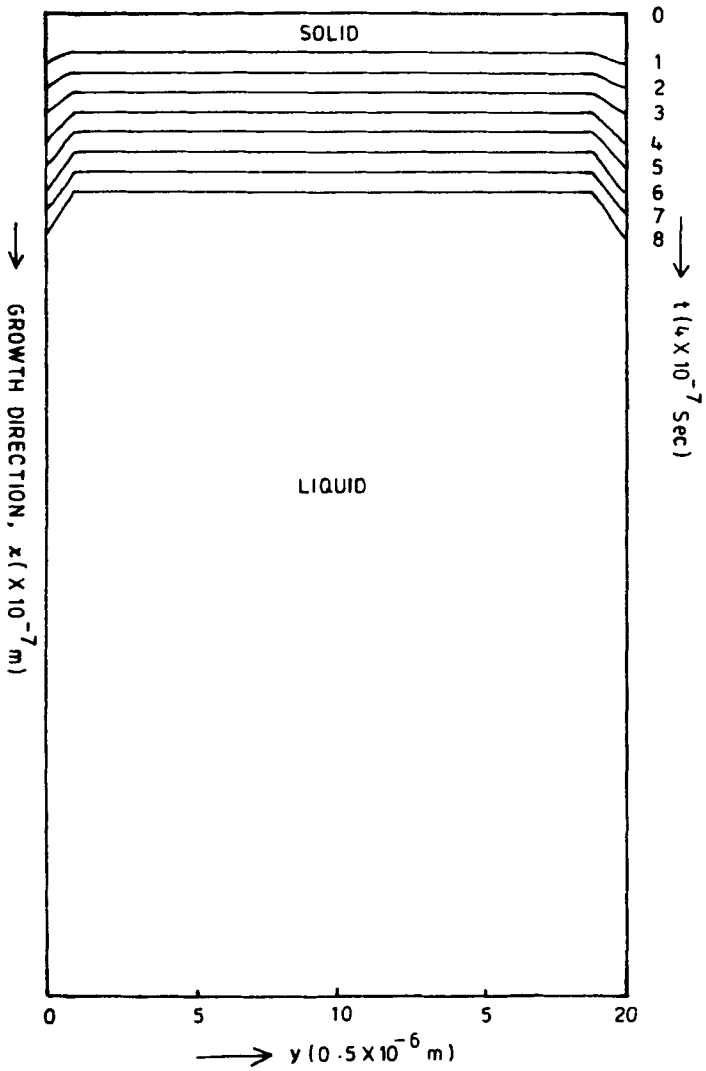

Figure 15(a). Time evolution of the solid–liquid interface for a system with $C_{L0} = 0{\cdot}3$, $T_1 = 1473$ K, $\Omega_L = 2{\cdot}8 \times 10^{-19}$ J/atom, $\Omega_S = 2{\cdot}8 \times 10^{-20}$ J/atom.

lowest at these points and concentrations C_{Lr} and C_{Sr} decrease at these points as shown in figures 7(c, d, e) respectively.

The corresponding plots for $X_r(y)$ with $C_{L0} = 0{\cdot}7$ are shown in figure 8(a). Kinks can be seen at points $2g$ and $4g$ and symmetrically at $16g$ and $18g$ indicating a possible formation of a dendrite tip. The temperature profile shows a sharp decrease and the rate

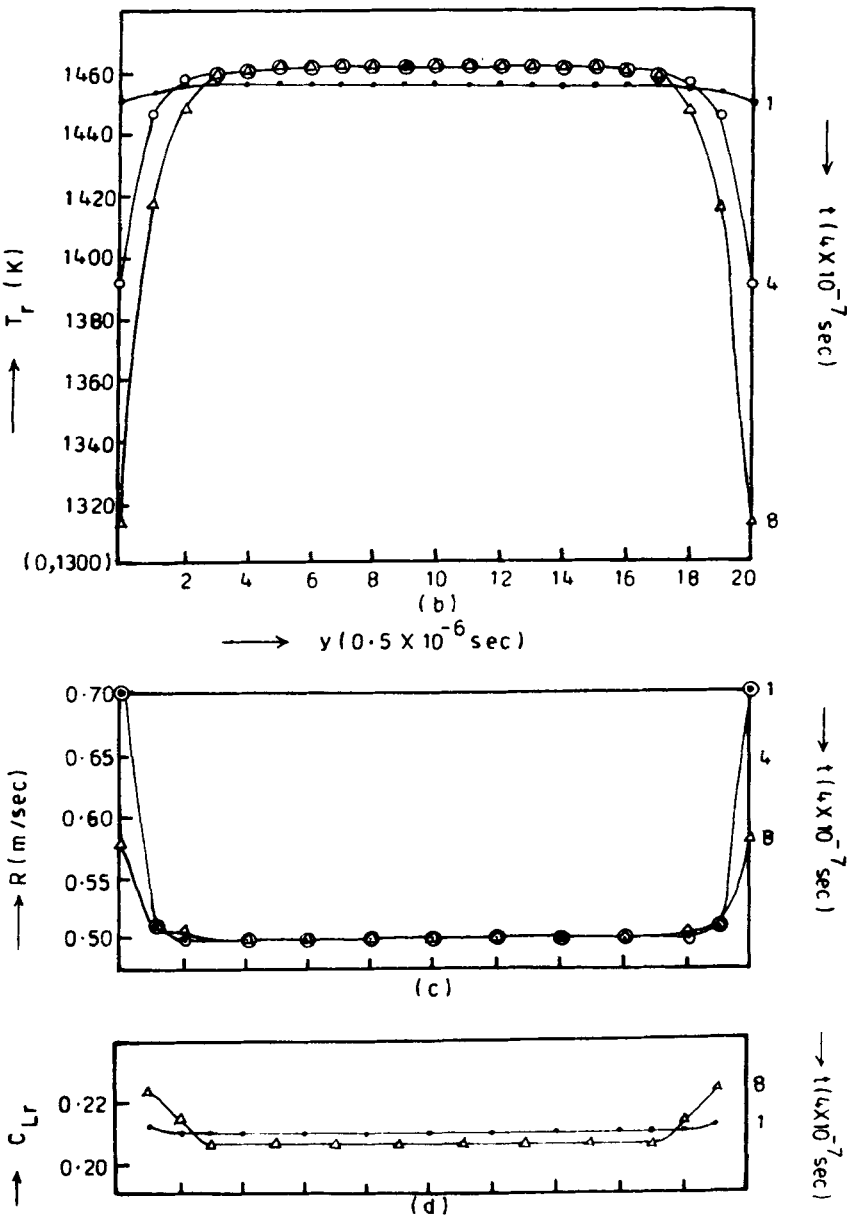

Figures 15(b–d).

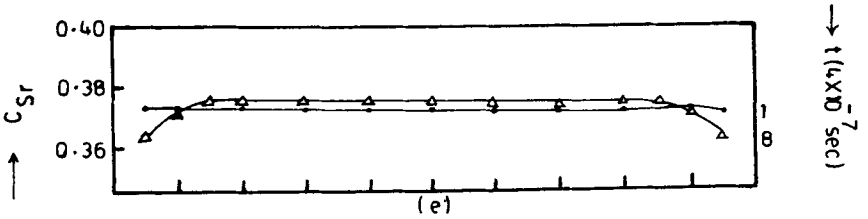

Figures 15(b–e). Time evolution of the interface: (**b**) temperature, (**c**) rate of growth, (**d**) concentration of the liquid phase, (**e**) concentration of the solid phase for a system with $C_{L0} = 0{\cdot}3$, $T_1 = 1473$ K, $\Omega_L = 2{\cdot}8 \times 10^{-19}$ J/atom, $\Omega_S = 2{\cdot}8 \times 10^{-20}$ J/atom.

profile shows a sharp increase at these points as shown in figures 8(b, c) respectively. C_{Lr} and C_{Sr} profiles show very small fluctuations about an average parabolic behaviour (figures 8(d, e)).

Figure 9(a) shows an even more complex structure of the interface. Temperature and rate of growth of this interface follow a similar trend as in case above and the concentrations on the interface surface are constant as shown in figures 9(b, c, d, e).

System II. The interface surface shown in figure 10(a) is nearly parabolic with curvature towards the solid phase and it exhibits a tendency to develop kinks near the middle of the sample. The temperature plots in figure 10(b) show considerable undercooling of the interface. The rate of growth decreases with time (figure 10(c)), which is characteristics of diffusion controlled growth. The concentration plots (figures 10(d, e)) show only small variations. The other shapes are shown in figures 11(a–e) to figures 14(a–e) for average liquid concentration $C_{L0} = 0{\cdot}25$, $0{\cdot}98, 0{\cdot}02$ and $0{\cdot}5$ respectively. An analysis of these curves depicts that the $X_r(y)$ shapes have the same characteristics for all C_{L0}, but the trends of T_r, C_{Lr}, C_{Sr} and R plots are reversed about $C_{L0} = 0{\cdot}5$.

System III. In this case the initially flat interface (figure 15(a)) retains its shape moving nearly equal distance in each time step except at the boundaries (edges) which are moving faster than the remaining points. The temperature plots show a cooling of the boundaries and the rate of growth plots show that the boundaries move slower than the other points. The liquid and the solid concentration curves are practically constant.

System IV. In figure 16(a) $X_r(y)$ is a parabolic surface with curvature towards the solid phase and boundaries move faster in the liquid phase. Temperature T_r, concentrations C_{Lr} and C_{Sr} surfaces evolve into parabolic shapes. The rate of growth profiles are also parabolic with curvature in a direction opposite to that of T_r, C_{Lr} and C_{Sr} plots. The evolution of surface for all time steps cannot be shown as their values lie close.

The $X_r(y)$, T_r, C_{Lr}, C_{Sr} and R plots for system V are similar to those obtained for system III and for system VI same patterns are obtained as for system II.

Thus it is seen from these plots that the radius of curvature of the solid–liquid interface changes during the solidification process and it also depends on the kinetic parameters

and the rate of cooling. Under conditions of slow growth in high temperature gradients planar interface growth occurs. It is believed that if the flux boundary condition is taken into account more rigorously while solving the four coupled equations, it might be possible to obtain dendrite, eutectic and cellular growth also.

The concentration of the solid phase varies and is different at different points and times. This shows that if the crystal is quenched at a particular time, a cross section of it will show the solid concentration variation as predicted by these calculations.

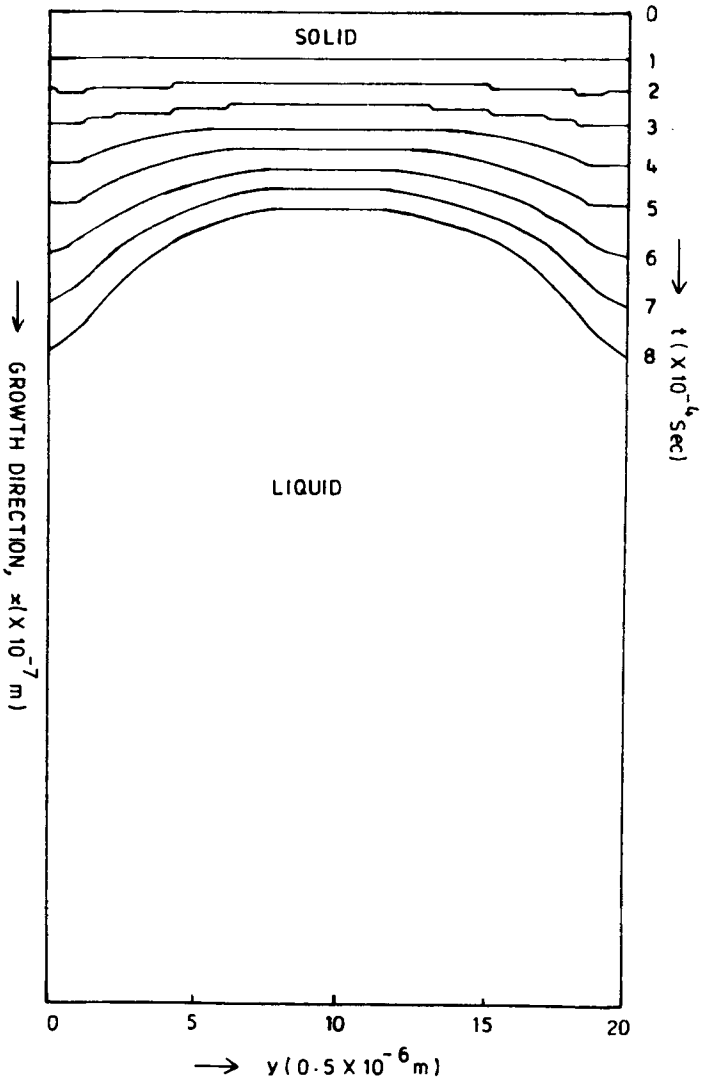

Figure 16(a). Time evolution of the solid–liquid interface for a system with $C_{L0} = 0{\cdot}5$, $T_1 = 1557\,\text{K}$, $\Omega_L = -2{\cdot}33 \times 10^{-20}\,\text{J/atom}$, $\Omega_S = -2{\cdot}47 \times 10^{-20}\,\text{J/atom}$.

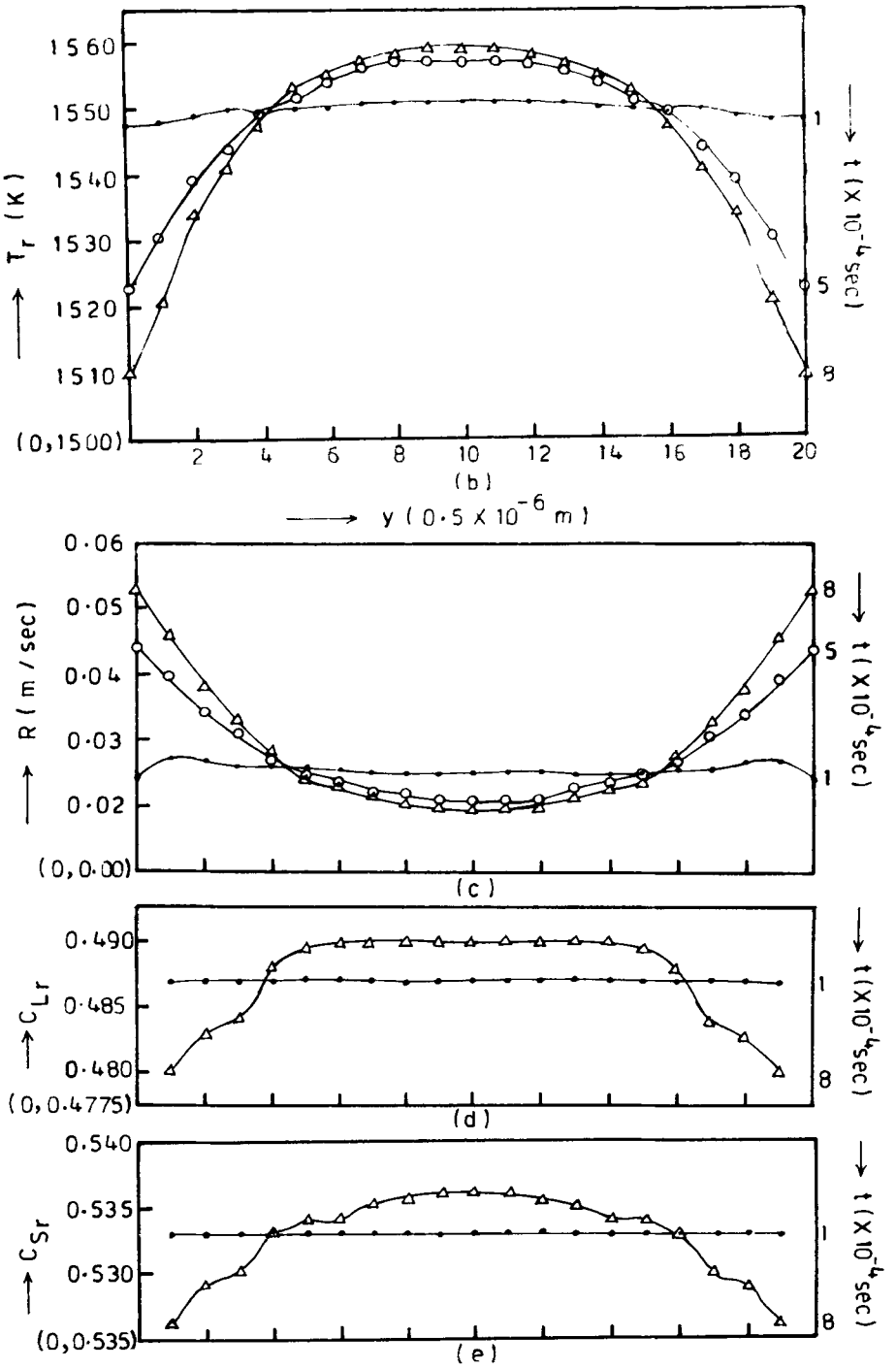

Figures 16(b–e). Time evolution of the interface: (**b**) temperature, (**c**) rate of growth, (**d**) concentration of the liquid phase, (**e**) concentration of the solid phase for a system with $C_{L0} = 0{\cdot}5$, $T_1 = 1557\,\text{K}$, $\Omega_L = -2{\cdot}33 \times 10^{-20}\,\text{J/atom}$, $\Omega_S = -2{\cdot}47 \times 10^{-20}\,\text{J/atom}$.

4. Conclusions

From the various results presented in §3 it is evident that phenomenon of solidification of binary melts can be studied comprehensively by using a stochastic model given in part I. These results qualitatively reproduce many of the phenomena observed experimentally, e.g., the phase diagrams obtained for various systems with different interaction parameters, effect of concentration and temperature on growth process, change of planar interface to various shapes.

Theories which neglect the kinetic processes at the solid–liquid interface [13] cannot be used for the systems in which the kinetic processes control the phase transition. Nonequilibrium solidification theories are more suitable to study crystal growth as during solidification the system is far from thermodynamic equilibrium.

The model presented here has been developed under an approximation that the system is not far from equilibrium. Nonequilibrium conditions are ascertained by high cooling rates of the order of 10^6–10^8 K/s. The rate of growth of the solid–liquid interface is time dependent, therefore the growth of the new phase is essentially under non-steady state conditions. During nonequilibrium solidification the concentrations of solid and liquid phases, rate of growth, undercooling and boundary conditions vary with time. These variations are included in this model enabling the determination of the composition and microstructure of the new phase. The various approximations can easily be relaxed in this model. However, a better explanation of the various interface shapes obtained can be given after considering the flux boundary condition more rigorously.

The model can be further extended to 4-dimensions (3-space, 1-time) and to multicomponent systems. Also, solution is obtained only for one type of boundary conditions which corresponds to crystal pulling technique of crystal growth. These boundary conditions can easily be modified to suit other experimental techniques.

References

[1] F C Flemings, in *Solidification processing* (Mc-Graw Hill Inc., New York, 1974)
[2] P Gordon, in *Principles of phase diagrams in materials* (Mc-Graw Hill, 1968; Jersey, 1972)
[3] A K Jena and M C Chaturvedi, in *Phase transformation in materials* (The Metals Society, Englewood Cliffs, New Jersey, 1992)
[4] B Caroli, C Caroli and B J Roulet, *J. Cryst. Growth* **66**, 575 (1984)
[5] Z Chvoj, *Cryst. Res. Technol.* **21**, 8, 1003 (1986)
[6] Z Chvoj, *Czech. J. Phys.* **B37**, 607 (1987)
[7] Z Chvoj, *Czech. J. Phys.* **B40**, 473 (1990)
[8] Z Chvoj, *Czech. J. Phys.* **B40**, 483 (1990)
[9] S Dass, *A stochastic approach to the study of solidification*, Ph.D. Thesis (Rani Durgavati University, 1994)
[10] S Dass, G Johri and L Pandey, *Pramana – J. Phys.* **47**, 447 (1996)
[11] C W Gardiner, in *Handbook of stochastic methods* (Springer-Verlag, Berlin, 1985)
[12] Z Chvoj, *Czech. J. Phys.* **B36**, 863 (1986)
[13] J S Langer and L A Turski, *Phys. Rev.* **A22**, 2189 (1980)